Nanostructured electrospun packaging incorporating functionalized emulsions with Mentha piperita L. essential oil: Study and application

J Lamarra
Centro de Investigación y Desarrollo en Ciencia y Tecnología de los Alimentos (CIDCA-CONICET- CIC-UNLP)
J Minnaard
Centro de Investigación y Desarrollo en Ciencia y Tecnología de los Alimentos (CIDCA-CONICET- CIC-UNLP)
M Medrano
Centro de Investigación y Desarrollo en Ciencia y Tecnología de los Alimentos (CIDCA-CONICET- CIC-UNLP)
D Lopez
Instituto de Ciencia y Tecnología de Polímeros, ICTP-CSIC
S Rivero
sandragmrivero@gmail.com

Centro de Investigación y Desarrollo en Ciencia y Tecnología de los Alimentos (CIDCA-CONICET- CIC-UNLP)
A Pinotti
Centro de Investigación y Desarrollo en Ciencia y Tecnología de los Alimentos (CIDCA-CONICET- CIC-UNLP)

Research Article

Keywords:

Posted Date: November 11th, 2025

DOI: https://doi.org/10.21203/rs.3.rs-7990047/v1

Additional Declarations: No competing interests reported.

Nanostructured electrospun packaging incorporating functionalized emulsions with *Mentha piperita* L. essential oil: Study and application

Lamarra J[1, 2], Minnaard J[1, 2], Medrano M[1], Lopez D[3], Rivero S[1, 2*], Pinotti A[1, 4]

[1]Centro de Investigación y Desarrollo en Ciencia y Tecnología de los Alimentos (CIDCA-CONICET-CIC-UNLP), Calle 47 y 116 S/N, La Plata Buenos Aires, Argentina

[2]Facultad de Ciencias Exactas, UNLP, 47 y 115 S/N, La Plata, Buenos Aires, Argentina

[3]Instituto de Ciencia y Tecnología de Polímeros, ICTP-CSIC, Calle Juan de La Cierva 3, 28006 Madrid, Spain

[4]Facultad de Ingeniería, UNLP, 47 y 115 S/N, La Plata, Buenos Aires, Argentina

*Corresponding author: Rivero S

sandragmrivero@gmail.com

Abstract

This study focused on the development of electrospun PVA-based nanofibers loaded with chitosan-stabilized *Pickering* emulsions containing encapsulated *Mentha piperita* L. essential oil. The Pickering emulsions were characterized by zeta potential, particle diameter and physical stability, whereas mat-forming solutions, prepared with different PVA:emulsion ratios, were evaluated for their rheological properties and electrospinnability. These PVA:emulsion ratios influenced fiber diameter, mechanical properties, and water resistance.

Controlled release was modeled in ethanol:water media with different polarities, which affected the release profile of the essential oil. Mats loaded with *Mentha piperit*a L. essential oil demonstrated good antimicrobial properties against *S. aureus*, both *in vitro* and when applied to a ham-based food model, supported by ATR-FTIR studies.

These results suggest that mats loaded with *Mentha piperita* L. may serve as promising candidates for antimicrobial food packaging applications.

Introduction

One of the great challenges today is the production of materials that exhibit varying functionalities depending on their intended applications. To address this issue, nanostructures with high surface-to-volume ratios have been developed through various techniques to enhance material efficiency and responsiveness (Liguori et al., 2022). Among the different synthesis methodologies, electrospinning is largely valuable to produce nanofibers. This technique applies a high-voltage electric field to a polymeric solution, generating a charged jet that undergoes rapid solvent evaporation, leading to the formation of continuous nanofibers (Salaris et al., 2022, Lamarra et al., 2020; Liguori et al., 2022). The matrix generated by electrospinning can be used in diverse applications, including controlled release of drugs, photodynamic therapy, and wound healing, among others (Nadaf et al., 2022). Due to the nanometric size of the fibers, their specific surface area and porosity make nanostructured materials highly suitable for the encapsulation of active compounds (Nadaf et al., 2022).

Poly(vinyl alcohol), a widely utilized polymer due to its biocompatibility and film-forming properties, is among the leading candidates for fiber formation by electrospinning (Lamarra et al., 2020; Morais et al., 2022; Panda et al., 2022) due to their good conductivity and water solubility. This biodegradable polymer is composed of vinyl alcohol units, with a proportion of residual acetate groups in its structure depending on the degree of hydrolysis (Lamarra et al., 2022).

The essential oil *Mentha piperita* (peppermint) is recognized for its numerous health benefits (Taylan et al. 2021). The main benefit relates to its antimicrobial capacity against pathogens such as *S. aureus, E. coli, and C. tropicalis* (Soltanbeigi et al., 2021). More precisely, Ashrafudoulla et al. (2023) demonstrated that peppermint essential oil exhibits antimicrobial activity against foodborne pathogens, including *Vibrio parahaemolyticus, Listeria monocytogenes, Pseudomonas aeruginosa, Escherichia coli O157:H7, and Salmonella typhimurium,* linking this effect to the capacity of menthol to disrupt cell membranes.

Mentha piperita contains high amounts of menthol and menthone, which were effective in inhibiting *S. aureus* both *in vitro* and in minced meat (Djenane et al., 2012). Concerning its antibacterial properties, *Mentha Piperita* essential oil was evaluated as an antibacterial agent in a chitosan-based packaging system, showing antibacterial capacity against bacteria that cause foodborne diseases (Mouhoub et al., 2022).

The low water solubility, the main limitation associated with the use of essential oils (EO), can be solved through the formation of emulsions. Emulsions are characterized by the predominance of surface interactions, allowing the coexistence of two immiscible phases, forming an oily phase dispersed in water (O/W emulsion) or a water phase dispersed in oil (W/O emulsion), achieved through the incorporation of amphiphilic molecules such as surfactants. A notable feature of emulsions is their thermodynamic instability (Piorkowski and Mc. Clements 2014).

Recently, the use of solid particles as alternatives to surfactants to stabilize emulsions has generated growing interest (Berton-Caratin and Schroen 2015; Fasihi et al., 2023; Ran et al., 2023). In this type of emulsion, referred to as *Pickering* emulsions, the nanoparticles located at the oil/water interface physically stabilize the dispersed droplets (Berton-Caratin and Schroen 2015; Sharkawy et al., 2020; Wu and Ma 2016). The advantage of these emulsions lies in the formation of a thicker interfacial layer, which enhances the stability of the emulsions compared to conventional surfactants (Berton-Carabin and Schroen 2015).

The nanoparticles used in the synthesis of *Pickering* emulsions must ensure good physical stability and, additionally, introduce extra functionalities such as antibacterial properties (Hadidi et al. 2020; Vahedikia et al., 2019). More precisely, one of the polymers that meets such requirements is chitosan. This biopolymer, a linear polysaccharide from deacetylated chitin, is a pH-responsive weak polyelectrolyte. Its charge density and surface adsorption adjust through amino group protonation, making it water-soluble below pH 6.5 and enabling adhesion to oppositely charged surfaces. Lai et al. (2021) developed a method to stabilize edible *Pickerin*g emulsions using silica nanoparticles modified with chitosan oligomers.

Ahmed et al. (2021) synthesized a stable chitosan-based *Pickering* emulsion and reported that its antibacterial activity against *S. aureus* increased with chitosan concentration. On the other hand, Hadidi et al. (2020) found that chitosan enhanced the antibacterial capacity of clove essential oil against strains of *S. aureus, E. coli, L. monocytogenes,* and *S. typhi,* indicating a synergistic effect between the polymer and the essential oil.

Among the possible applications of these emulsions, food preservation deserves to be mentioned. For example, Fasihi et al. (2023) described a film-based material with *Pickering* emulsions encasing ginger essential oil. This material showed good preservation capacity to preserve bread slices and significant antimicrobial activity against *Penicillium digitatum*. Furthermore, Ran et al. (2023) investigated collagen films loaded with *Pickering* emulsions based on cinnamon essential oil, which demonstrated antimicrobial properties against various pathogens and extended the shelf life of pork.

This study focuses on the development of poly(vinyl alcohol) based nanofibers loaded with *Pickering* emulsions encapsulating peppermint essential oil. The resulting *Pickering* emulsion (PE) was characterized by zeta potential, particle size, and physical stability. Rheological properties, as well as microstructural characteristics by scanning electron microscopy (SEM), were analyzed considering the ratio of PVA to emulsion.

The mechanical properties of the mats were assessed, and the controlled release of peppermint EO was analyzed using food stimulants. Finally, the antimicrobial efficacy of the active matrix was assessed against *Staphylococcus aureus* and *Escherichia coli*, both through *in vitro* assays and following its application to a ham used as a model food matrix.

2. Materials and methods

2.1 Materials

Chitosan (CH, PMv=6.76x10^5 Da, with a deacetylation degree of 90%) was supplied by Parafarm® (Argentina), whereas poly(vinyl alcohol) (PVA), characterized by a hydrolysis degree of 86–89 % and molecular weight range of 50 to 55 kDa, was acquired from Dupont (USA). Sodium dodecyl sulfate (SDS, Cicarelli, Argentina) was used as a surfactant agent. Analytical grade sodium tripolyphosphate (TPP) was obtained from Anedra (Argentina). Additionally, *Mentha piperita* essential oil (EO) was purchased from Esencias del Bosque (La Plata, Argentina).

2.2 Methods

2.2.1 Synthesis and characterization of Pickering emulsions

For the formation of *Pickering* emulsions, a solution of CH was prepared at a concentration of 0.75% (w/v) in acetic acid at 0.75% (v/v). This solution was then compatibilized with a poly(vinyl alcohol) (PVA) solution at 0.75% (w/v). Sodium dodecyl sulfate (SDS) was incorporated as a surfactant to a final concentration of 1g/L. Subsequently, peppermint (*Mentha piperita*) essential oil was added drop by drop, reaching a final concentration of 7.5% (v/v) by homogenization at 21500 rpm using an Ultraturrax T-25 (Janke and Kunkel, IKA-Labortechnik, Germany) for 10 min. To reduce the droplet size of the pre-emulsion, it was subjected to a microfluidization process of 4 cycles at 1000 bar. Following this, sodium tripolyphosphate (TPP) was added drop by drop until a concentration of 0.15% (w/v) was reached. The obtained *Pickering* emulsion (PE) underwent 6 additional homogenization cycles, 4 at 1000 bar and 2 at 1200 bar. As a control, the formulated suspension (S) without the incorporation of essential oil was used.

The synthesized suspension (S) and emulsion (PE) were characterized by zeta potential (ZP) and hydrodynamic diameter (D_h) by using a nanoparticle analyzer Horiba Scientific Equipment-Model SZ-100Z (Horiba, Ltd., United Kingdom). The zeta potential was assessed through carbon cells specific to this equipment, whereas the hydrodynamic diameter was determined by dynamic light scattering (DLS) using a diode laser (532 nm) and a detection angle of 173°.

The global physical stability of *Pickering* emulsions was evaluated using light scattering with a vertical scan analyzer (QuickScan, Beckman Coulter, Fullerton, USA) at room temperature following a procedure like that outlined by Lamarra et al. (2020). Briefly, synthesized suspension (S) and emulsion (PE) were placed into cylindrical test tubes and scanned from the bottom to the top with monochromatic radiation at a wavelength of 800 nm, recording the backscattering profile over several days.

2.2.2 Formation of fiber-forming suspensions

A 16% (w/v) solution of PVA was prepared by dissolving the polymer in water at 90 °C for 5 h. Then, the previously formed PVA solution was mixed with different proportions of PE for 3 h at room temperature. The resulting fiber-forming solutions were classified based on the PVA/PE ratios of 4:1, 3:1, and 2.5:1.

2.2.3 Rheological properties

A TA Instruments HR20 rheometer (TA, Instruments, USA) was used to evaluate the rheological behavior of the fiber precursor solutions. The tests were conducted with a plate-plate detector with a diameter of 40 mm and a gap of 1000 µm. Rheological behavior was mathematically fitted by using the Ostwald de Waele model, and in the case of non-Newtonian systems, apparent viscosity was calculated at 400 s^{-1}. The viscoelastic behavior of the samples was studied through dynamic assays. To determine the linear viscoelasticity range, a stress sweep (from 10^{-9} to 10^{-4} Pa) at constant frequency (1 Hz) was performed. Additionally, frequency sweep tests ranging from 0.01 to 100 Hz were performed under a constant stress of 1 Pa. The measured dynamic rheological parameters included the storage modulus (G'), the loss modulus (G"), and the damping factor (tan δ), calculated as the ratio G"/G'. Mechanical spectra were constructed by plotting G' and G" against the angular frequency (ω).

Rotational and frequency sweep tests were carried out on the different samples at 25°C. Each rheological test was performed in at least two replicates.

2.2.4 Nanofiber formation by electrospinning

The formation of nanofibers was carried out using an electrospinning Spinbox model supplied by Bioinicia® (Bioinicia Fluidnatek SLU, Valencia, Spain) operating at 24 kV, a flow of 0.4 mL h^{-1}, and a needle-collector distance of 17 cm. The average collection time of the nanostructures obtained by electrospinning average time was 18 h.

2.2.5 Morphological analysis by SEM

The microstructure of the mats was analyzed by scanning electron microscopy (SEM) using an FEI model Quanta 200 microscope (FEI Company, The Netherlands). The specimens were examined at an acceleration voltage of 15 kV. Fiber diameters were calculated using the Fiji program (Image J, NIH, USA).

2.2.6 Microstructure by ATR-FTIR

Fourier transform infrared spectroscopy equipment (Nicolet, iS10 ThermoScientific, Madison, USA) was used in the attenuated total reflectance mode (Smart iTX accessory). The data recorded in the range of 400–4000 cm^{-1} by accumulation of 32 scans with a resolution of 4 cm^{-1} were analyzed using Omnic 8 software (ThermoScientific).

2.2.7 Mechanical properties

The mechanical properties of the mats were evaluated using a TA.XT2i-Stable Micro Systems (England) texturometer. The mat probes were stretched with a tension grip system A/TG at a constant rate of 0.5 mm s^{-1}. Texture Expert Exceed software was used to record the force curve (N) as a deformation function (mm) to calculate elongation at break (ε), maximum tensile strength (TS), and tenacity (T).

2.2.8 Water resistance properties

The moisture was measured by drying the samples under vacuum at 60 ^{o}C until constant weight. Water solubility and swelling were evaluated by dipping the mats in water for 1 h. To calculate the swelling, the mats were dried with paper and weighed in an analytical balance; meanwhile, to evaluate the solubility, the samples were dried under vacuum at 60 ^{o}C until constant weight.

2.2.9 Controlled release

For evaluating the materials as a potential controlled release dispositive, different assays were carried out in different simulant media such as 25% ethanol (aqueous media), 50% ethanol (partially lipid food media), and 75% ethanol (lipid food simulant media). Mats of 2×2 cm^2 were cut and placed in the release media. To quantify the amount of EO release, aliquots of 1 mL were withdrawn, adding 1 mL of fresh media each time. The EO concentration was quantified using a spectrophotometer (Uvmini-1240, Shimadzu) measuring at 237 nm, a wavelength at which key monoterpenes such as menthol exhibit characteristic absorbance (Kamatou et al., 2013).

2.2.10 Antibacterial properties

Bacterial strains and culture conditions

Staphylococcus aureus ATCC 6538 and *Escherichia coli* ATCC 25922, preserved at -80°C, were reactivated in nutritive broth at 37°C for 24 h. Fresh nutritive broth was then inoculated with 2% (v/v) of the reactivated cultures. After incubation for 18-24 h at 37°C, the cultures were centrifuged at 3600 x g and the pellets were resuspended in the same medium. The optical density (DO) at 600 nm was measured using a spectrophotometer (Metrolab Argentina), and the bacterial suspensions were adjusted to an OD of 0.3, corresponding to approximately 1×10^7 CFU/mL) for use in the antimicrobial activity assay.

Antimicrobial activity *in vitro*

Three mL of *Staphylococcus aureus* and *Escherichia coli* bacterial suspensions (OD = 0.3 in nutritive broth) were placed into sterile 3 mL Eppendorf tubes. Mats of 2 cm diameter were introduced into the bacterial suspensions and incubated at 20°C and 30°C for 24 h and 48 h. After that, serial dilutions in tryptone 0.1% w/v (Biokar, Paris, France) were conducted, and the proper dilutions were inoculated in Plate Count Agar (PCA) (Biokar, Paris, France). The plates were incubated at 37°C for 24–48 h, and colonies were counted. Results were expressed in CFU mL^{-1}. Conditions were assayed in triplicate. Three independent experiments were conducted.

Antibacterial assay by ATR-FTIR spectroscopy

ATR-FTIR spectroscopy was used to determine changes in bacterial structure after exposure to PVA/S and PVA/PE matrices, applying the film technique described by Naumann (2006) and Leung et al. (2016).

After taking samples for plate counting, PVA/S and PVA/PE mats that had been in contact with bacterial suspensions were removed. The cells were collected by centrifugation at 10,000 rpm for 10 min in 1.5 mL Eppendorf tubes, and the supernatant was discarded. The cells were then resuspended in Milli-Q grade water, and aliquots of 100 µL of the concentrated bacterial suspension were spread on the surface of a diamond ATR crystal and dried to obtain transparent films. Spectra were acquired, baseline offset correction was performed, and the obtained data set was analyzed using OMNIC software.

Antimicrobial activity challenge: Food application of nanostructured active mat

A slice of ham (Bocatti, Argentina) obtained from a local store (average weight 3.985 ± 0.175 g) was cut into pieces using a sterile cork borer. The ham pieces were placed between two nanostructured mats (one on top and another on the bottom), some with EO and without, in triplicate. A control with synthetic film (nylon) and a control without any film were also included. The pieces without films were then placed in sterile Petri dishes and incubated at 4 °C for 48 h. After that, each piece was transferred to sterile plastic bags (Whirl-Pak, USA) and homogenized for 1 min at high speed in a Seward Stomacher (Model 400; West Sussex, United Kingdom) in a 1:10 dilution with sterile peptone water 0.1 % w/v. Appropriate dilutions of each sample were placed on Plate Count Agar (PCA) (Biokar) and Baird Parker agar (Biokar) supplemented with 50 mL L^{-1} of 50% egg yolk-saline emulsion and 10 mL L^{-1} of 1% potassium tellurite solution (Britania, Argentina). The plates were incubated at 37°C for 24–48 h, and colonies were counted. Results were expressed in CFU g^{-1}. Three independent trials were conducted.

2.2.11 Statistical analysis

For the statistical analysis of the results, the statistical InfoStat v2009 software (Argentina) and GraphPad Prism 9 (GraphPad Software Company, CA, USA) were applied. Analysis of variance was carried out by means of ANOVA procedures followed by Fisher LSD test for simultaneous pairwise comparisons. F-tests and differences in means were considered statistically significant when $p<0.05$. Data were expressed as the mean ± standard deviation (SD) unless otherwise stated. Assumptions of normality and homogeneity of variances were considered in all analyses.

3. Results and discussion

3.1 Characterization of *Pickering* emulsion

Table 1 summarizes the values of zeta potential (ZP) and hydrodynamic diameter (Z_{av}) of the *Pickering* emulsions with peppermint EO (PE) and the suspension without EO (S).

Table 1. Characterization of systems with *Mentha piperita* EO (PE) and without EO (S) through zeta potential and particle diameter

Sample	**ZP (mV)**	**Z_{av} (nm)**	**PI**	**TSI (%)**
S	27±4[a]	290±38[a]	0.5[a]	0.0017[b]
PE	63±1[b]	427±19[b]	0.5[a]	0.0008[a]

[a,b] Different superscripts within the same column indicate significant differences between samples ($p<0.05$).

The ZP values for both systems were found to be positive, due to the presence of excess polycation (chitosan), indicating that both exhibited good stability, as their ZP values exceeded +30 mV (Lamarra et al., 2016). The comparison of the suspension and the charged emulsion revealed that the addition of peppermint EO resulted in a higher surface charge ($p<0.05$). This result could be explained by findings from Wu et al. (2022), who reported that when forming *Pickering* emulsions based on gliadin for encapsulating methyl jasmonate, the presence of the latter increased the surface charge due to the interaction between the active compound and gliadin, which prevented flocculation caused by gliadin-gliadin interactions.

Examining the average diameter (Z_{av}) values presented in Table 1, it was observed that chitosan particles complexed with SDS exhibited a size of 290 nm. This finding aligns with the results informed by Bezrodnykh et al. (2021), who stated that particle size depends on several factors, including molecular weight and anion concentration. Conversely, the *Pickering* emulsion displayed a size of 427 nm, which was larger than that of the nanoparticles. This phenomenon is a logical consequence of the requirements for nanoparticles to effectively stabilize emulsions, since their diameters must be sufficiently small to cover the surface of the oil droplets (Niu et al., 2022). Furthermore, Low et al. (2020) reported a direct proportional relationship between the nanoparticle sizes and the diameter of EO droplets.

3.2 Rheological properties

Assessing rheological properties is essential for determining electrospinnability, as these properties correlate with the morphology characteristics of nanofibers obtained (Javaid et al., 2022; Wu et al., 2023; Zhang et al., 2023). Viscosity is one of the key flow parameters used to evaluate rheological performance (Zhang et al., 2023).

Table 2 summarizes the values of apparent viscosity determined for the samples studied.

As can be seen in Table 2, the control sample of PVA 14% w/v exhibited the highest viscosity, a phenomenon attributed to the equilibrium configurations of hydrogen bonding interactions among the –OH groups along the PVA chains and between polymer chains and water molecules (Morais et al., 2023).

On the other hand, the incorporation of the suspension without EO resulted in a reduction of viscosity, suggesting that the interaction between the polymeric chains was disrupted. These results correlated with the observations reported by Chen et al. (2022), who evaluated the effect of chitosan concentration on PVA solubilized in different solvents. These authors informed that the addition of chitosan produces a decrease in viscosity, thus affecting the fiber-forming capacity during the electrospinning process. Additionally, the functionalized emulsion with EO in the same proportion produced a moderate increase of 56% in viscosity, possibly due to interactions between the poly(vinyl alcohol) matrix and EO (Tampau et al., 2020). Analyzing the concentration of the active emulsion (Table 2), an increase in concentration led to a decrease in viscosity, a result consistent with our previous studies (Lamarra et al., 2020; Lamarra et al., 2023). This phenomenon may be attributed to the dilution of the PVA caused by the addition of the active emulsion (assuming affinity between the phases of the system), which reduced the entanglement of polymeric chains (Wu et al., 2023).

The Ostwald de Waele model was used to fit the experimental curves (Morais et al., 2023) according to the following Equation:

$$\tau = \boldsymbol{K}\,\gamma^{n} \qquad [1]$$

Where τ is the shear stress, K is the consistency index, which measures the liquid´s resistance to flow, and n is the flow index, which indicates the degree of deviation from the Newtonian behavior.

Table 2. Ostwald de Waele parameters and apparent viscosity values of different precursor solutions

Samples	$\eta_{400\ s^{-1}}$ (Pa.s)	K (Pa.s)	n	R^2
PVA	4.30^e ±0.10	24.0^d ±7	0.72^a ±0.05	0.9934
PVA/S 4:1	1.56^b ±0.08	4.3^b ±0.5	0.84^{b,c} ±0.01	0.9991
PVA/PE 4:1	2.29^d±0.01	7.0^b ±1.0	0.80^b ±0.03	0.9985
PVA/PE 3:1	2.07^c ±0.02	6.4^b ±0.01	0.81^b ±0.01	0.9988
PVA/PE 2.5:1	1.14^a±0.02	2.5^b ±0.3	0.87^c ±0.01	0.9994

^{a,b} Different superscript letters within the same column indicate significant differences between treatments ($p<0.05$).

The consistency index followed a similar trend to that observed in viscosity values. The control sample exhibited the lowest n value, corresponding to the highest viscosity value reported. These flow index values can provide an estimation of the processing capacity of the samples by electrospinning, considering that when n=1, fiber formation did not occur, while an excessively low n value may hinder flow. In this context, Zhang et al. (2023) stated that values equal to or higher than 0.6 indicate solutions with the potential for electrospinning processing. All samples exhibited n values below 1, suggesting shear-thinning behavior, which implies that as the shear rate increases, the chain entanglement is less than the disentanglement (Zhang et al., 2023).

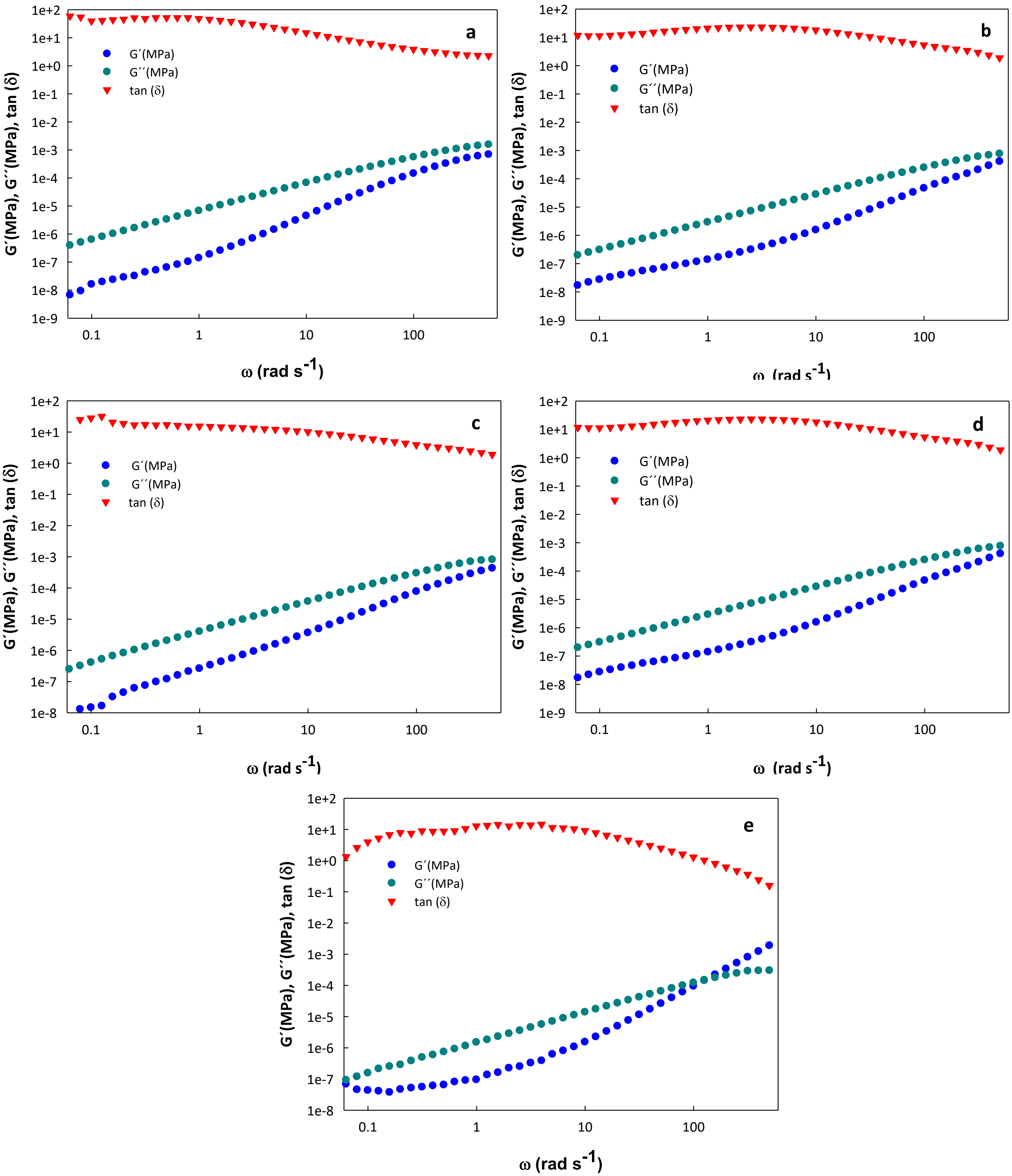
a
G´(MPa)
G´´(MPa)
tan (δ)
G´(MPa), G´´(MPa), tan (δ)
1e+2
1e+1
1e+0
1e-1
1e-2
1e-3
1e-4
1e-5
1e-6
1e-7
1e-8
1e-9
0.1
1
10
100
ω (rad s-1)
b
G´(MPa)
G´´(MPa)
tan (δ)
G´(MPa), G´´(MPa), tan (δ)
c
G´(MPa)
G´´(MPa)
tan (δ)
G´(MPa), G´´(MPa), tan (δ)
ω (rad s-1)
d
G´(MPa)
G´´(MPa)
tan (δ)
G´(MPa), G´´(MPa), tan (δ)
ω (rad s-1)
e
G´(MPa)
G´´(MPa)
tan (δ)
G´(MPa), G´´(MPa), tan (δ)
ω (rad s-1)

Figure 1. Dynamic rheology test of the samples: **a)** PVA, **b)** PVA/S 4:1 (without peppermint EO), **c)** PVA/PE 4:1, **d)** PVA/PE 3:1, and **e)** PVA/PE 2.5:1.

The flow index trends indicated that there were no significant differences between the samples without EO and with EO in the 3:1 proportion. However, an increase in the concentration of the active emulsion (2.5:1) led to a rise in this index, indicating a transition toward a more Newtonian-like behavior (Morais et al., 2023; Chen et al., 2022).

Complementarily, a dynamic rheological test was carried out for a more precise rheological assessment of the electrospinnable solutions (Figure 1). According to Zhang et al. (2023), when a polymer sample is submitted to an electrical field, the application of a periodic force in a rheological evaluation can effectively replicate stress and strain behavior.

As can be observed in Figure 1, the loss or viscous modulus (G´´) exhibited higher values than the storage or elastic modulus (G´) across a broad range, indicating the viscoelastic behavior of samples with a predominance of viscous flow (Zhang et al., 2023). This observation was also reflected in the loss factor (tan (δ)), which establishes a relationship between G´´and G´. Similar results were reported by Liu et al. (2015), who explained that both the viscous and elastic moduli showed an increase in response with rising angular frequency. According to Liu et al. (2022) and Liu et al. (2015), the approximation of the elastic and viscous moduli or the existence of crossover points between G′ and G″ is an indicator of a solution's electrospinnability. Thus, it reflects the presence of a sufficiently stable entanglement network (Liu et al., 2022). In polymer solutions, viscoelastic behavior is largely governed by such networks or by similar topological constraints.

When the tan(δ) value is greater than 1, the material shows a viscous flow, while a value lower than 1 indicates a predominantly elastic behavior. If tan(δ) equals 1, the system reaches the gel point, a state between solid and liquid. Two critical characteristics for processing the samples are associated with the working, which must ensure viscous flow behavior and distance from the gel point (Zhang et al., 2023). As noted by Serpelloni et al. (2024), a predominance of liquid behavior over elastic behavior is desirable to produce uniform fibers. This suggests these samples are promising candidates for electrospinning.

3.3 Microstructure by SEM

Figure 2 depicts the SEM micrographs of different samples.

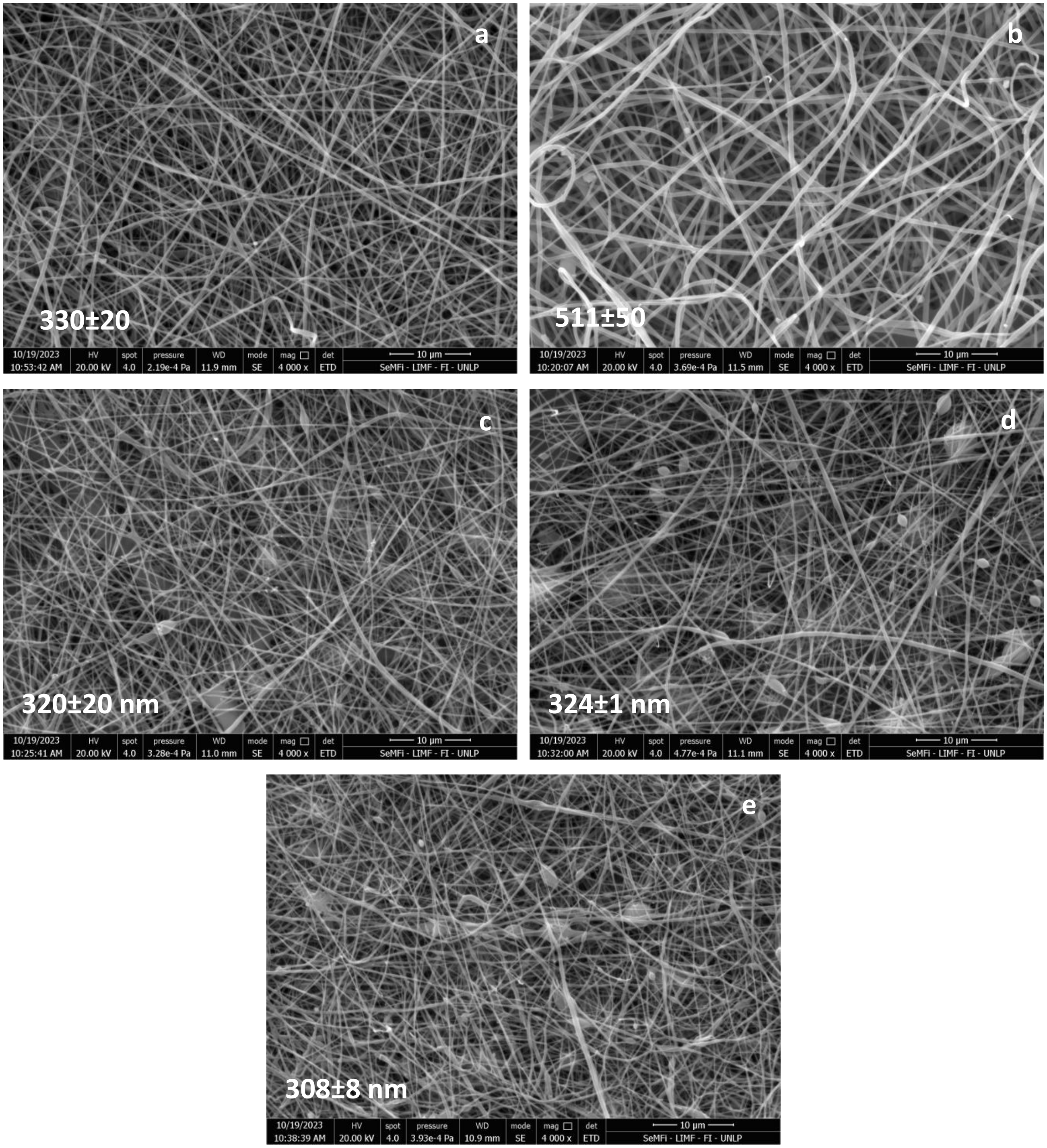

Figure 2. SEM micrographs of nanofibers formulated with a) PVA, b) PVA/S 4:1, c) PVA/PE 4:1, d) PVA/PE 3:1, and e) PVA/PE 2.5:1. Magnification and average diameters (with the corresponding standard deviation) are indicated in the micrographs.

As can be seen in Figure 2, the PVA matrix exhibited homogeneous fibers without the appearance of beads in their structure, with an average diameter of 330 nm. The uniformity of these fibers resulted from the effective entanglement of polymer chains (Wu et al., 2023). In contrast, the inclusion of the suspension without EO produced wider fibers, with an average diameter of 511 nm, indicating an increase in this parameter compared to the control matrix, despite a reported decrease in viscosity. A similar fact was explained by Jiang et al. (2024), who indicated that the inclusion of silver and zinc nanoparticles led to higher drawing resistance due to the interactions between the nanoparticles and the polymeric matrix at the interphase level, increasing the fiber diameter. Additionally, it is important to highlight that the decrease in conductivity observed in the absence of EO (sample PVA-S 4:1) resulted in an increase in fiber diameter, which can be explained by insufficient jet elongation (de Oliveira Mori et al., 2014). An increase in solution conductivity with higher EO proportions leads to a reduction in fiber diameter, attributed to the greater surface charge density on the jet, which enhances the elongational force acting during its trajectory toward the collector.

The conductivity plays a critical role in the electrospinning process, as higher conductivity allows the solution to carry more electric charges. This improvement induces greater stretching of the polymer jet under the electric field, which typically results in thinner, more uniform fibers with reduced bead formation (Erdem & Akalın, 2015).

The addition of active emulsion in different proportions produced matrices with diameters statistically similar to the control ($p>0.05$). However, an increase in emulsion proportion caused an increase in the number of beads, a phenomenon linked to the reduction in viscosity of the system, which may be attributed to a plasticizing effect from the incorporation of EO (Unalan et al., 2019).

3.4 ATR-FTIR analysis

The ATR-FTIR spectra were analyzed to achieve a microstructural study of the obtained mats. Two spectral regions were considered, which exhibited characteristic peaks of the base polymer (PVA). The first spectral region, ranging from 3700 to 3000 cm^{-1} (Figure 3a) contains the band associated with the stretching of –OH groups. In the presence of EO, it resulted in a red shift, suggesting the formation of more intense or more numerous hydrogen bonds (Tu et al., 2008).

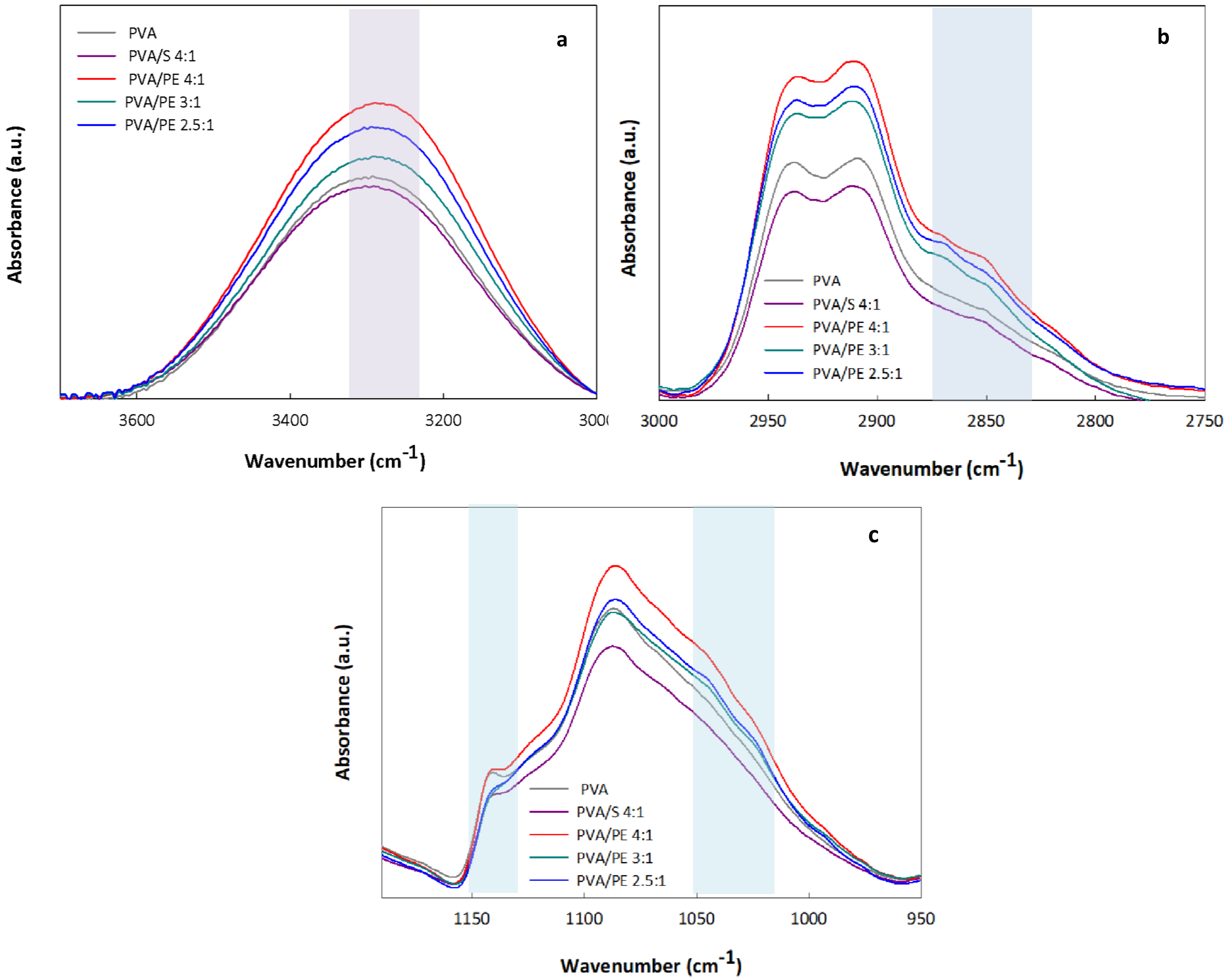

Figure 3. ATR-FTIR spectra of electrospun matrices functionalized with diverse proportions of *Mentha piperita* essential oil showing different regions: a) 3600 -3000 cm^{-1}, b) 3000-2700 cm^{-1}, and, c) 1150-950 cm^{-1}.

Additionally, the spectral region between 3000 and 2700 cm^{-1} was examined (Figure 3b). In this window, the vibrational mode related to the stretching of methyl groups was identified (Lamarra et al., 2022). The presence of peppermint EO caused the emergence of peaks around 2850 and 2860 cm^{-1}, which are associated with the essential oil encapsulation within the matrix.

At 1414 cm^{-1}, the signal indicative of the interactions between the PVA and chitosan affected the C-H vibrational motion of the PVA band (Perez-Calderon et al., 2023). Similarly, a modification in the band at 1144 cm^{-1}, attributed to the C–O stretching of the crystalline sequence of PVA, was observed, along with the appearance of shoulders at 1044 and 1021 cm^{-1} (Figure 3c).

3.5 Mechanical properties

Table 3 summarizes the tensile strength, percentage of elongation, and tenacity of different electrospun matrices.

Table 3. Mechanical properties of different electrospun matrices of PVA-based electrospun mats formulated without (PVA/S 4:1) and with *Mentha piperita* essential oil (PVA/PE)

Sample	Tensile strength (MPa)	Elongation (%)	Tenacity (J)
PVA	$4.4^{a}\pm0.9$	$12^{c}\pm2$	$0.028^{c}\pm0.006$
PVA/S 4:1	$5.2^{a}\pm0.9$	$15^{d}\pm1$	$0.037^{d}\pm0.007$
PVA/PE 4:1	$5.0^{a}\pm1.0$	$16^{d}\pm0.8$	$0.032^{d}\pm0.005$
PVA/PE 3:1	$6.6^{b}\pm0.9$	$4.3^{a}\pm0.8$	$0.013^{a}\pm0.002$
PVA/PE 2.5:1	$8.6^{c}\pm0.9$	$2.6^{b}\pm0.6$	$0.018^{b}\pm0.003$

[a,b,c,d] Different superscripts within the same column indicate significant differences between treatments ($p<0.05$)

The evaluated mechanical properties, as summarized in Table 3, were influenced by the quantity of emulsion used. Initially, the addition of both active emulsions and suspension at the lowest ratio (4:1) did not produce significant changes in the tensile strength values compared to the control mat, while the elongation increased significantly ($p<0.05$). Furthermore, an increase even greater (3:1 and 2.5:1) in the content of the *Pickering* emulsion correlated with enhanced tensile strength values and the consequent decrease in elongation, which also manifested changes in the tenacity values. The observed increase in elongation at the lower percentage of emulsion can be attributed to the effective dispersion of the *Pickering* emulsion within the PVA matrix. In contrast, a higher concentration of emulsion may lead to the agglomeration of emulsion droplets within the matrix, adversely affecting its mechanical properties (Cheng et al., 2017). In addition, the increase in interactions, together with the synergistic effect promoted by the higher chitosan and essential oil content, and the greater proportion of emulsion, contributed to the enhanced properties, further supported by the cross-linking or reinforcing role of *Pickering* emulsions.

These effects due to hydrogen bonds may be attributed to interactions between PVA and EO as demonstrated by ATR-FTIR spectra. The tenacity decreased with increasing emulsion content, indicating that the presence of active emulsion and, therefore, EO led to diminished energy dissipation at the breaking point (Milanesi et al., 2021). This was linked to the reduced elongation of these samples compared to the control.

In this sense, Das et al. (2023) reported that an increase in the concentrations of hydroxypropyl-β-cyclodextrin and atrazine complexes in PVA mats led to higher strength and elastic modulus but lower elongation. This phenomenon was attributed to strong hydrogen bonding interactions between the complex and PVA. These bonds restricted polymer chain mobility and reduced average elasticity. Based on the mechanical performance, the sample PVA-PE 4:1 was selected to study water affinity properties and for food matrix application of this material, while the PVA-S 4:1 sample was used as a control.

3.6 Water-resistance properties

Table 4 summarizes the water-resistance properties of electrospun mats with and without EO.

As can be seen in Table 4, moisture values between mats with and without EO were not significantly different. On the other hand, low moisture content is crucial to retard the bacterial growth (Gaikwad et al. 2019). The mat containing EO exhibited significantly lower solubility values compared to those without the active agent, with statistically significant differences observed between samples ($p<0.05$). This behavior could be due to interactions between the PVA matrix and chitosan (Garavand et al., 2022; Çay et al., 2014). In addition, the findings obtained could be explained by the inclusion of hydrophobic compounds, thereby preserving the mat's structure in an aqueous environment (Kong et al., 2022).

Similarly, the swelling percentage decreased with the inclusion of the EO-loaded emulsion, which may be due to the hydrophobic nature of EO and the improved structural integrity of the matrix (Kavoosi et al., 2014; Ardekani et al., 2019). According to Gahruie et al. (2017), the network strengthening can be induced by extensive hydrogen bonds between the polymer backbone and polar head groups of surfactant molecules present at the interface of dispersed nanodroplets.

Table 4. Water-resistance properties of PVA-based electrospun mats formulated without (PVA/S 4:1) and with *Mentha piperita* essential oil (PVA/PE 4:1)

Sample	Moisture (%)	Solubility (%)	Swelling (%)
PVA/S 4:1	$6.3^{a}\pm0.2$	$61.3^{b}\pm0.5$	$233^{b}\pm45$
PVA/PE 4:1	$6.4^{a}\pm0.8$	$18.7^{a}\pm0.6$	$119^{a}\pm8$

^{a,b} Different superscripts within the same column indicate statistically significant differences between samples ($p<0.05$)

3.7 Controlled release

Figure 4 depicts the controlled release of the active agent in various solvents. The medium containing equal amounts of ethanol and water exhibited the highest release percentage, while the more hydrophilic medium (ethanol-water 25:75) demonstrated the lowest dosage release. Similar results were reported by Lamarra et al. (2020) for systems with comparable characteristics, indicating that the highest release percentage in the 50% ethanol medium resulted from a combination of two processes, the peppermint EO solubility was favored by its affinity for ethanol and by swelling of the matrix, which was attributed to the hydrophilic nature of the polymers that constitute the system. Overall, the release percentage was relatively low, with the maximum being 20%. This observation contrasted with the findings of Costa et al. (2019), who affirmed that controlled release in the electrospun matrix is significant due to the large specific surface area characteristic of this type of matrix. Additionally, the lower controlled release percentage may be attributed to intermolecular interactions between the PVA matrix and the essential oil, as described in the ATR-FTIR results.

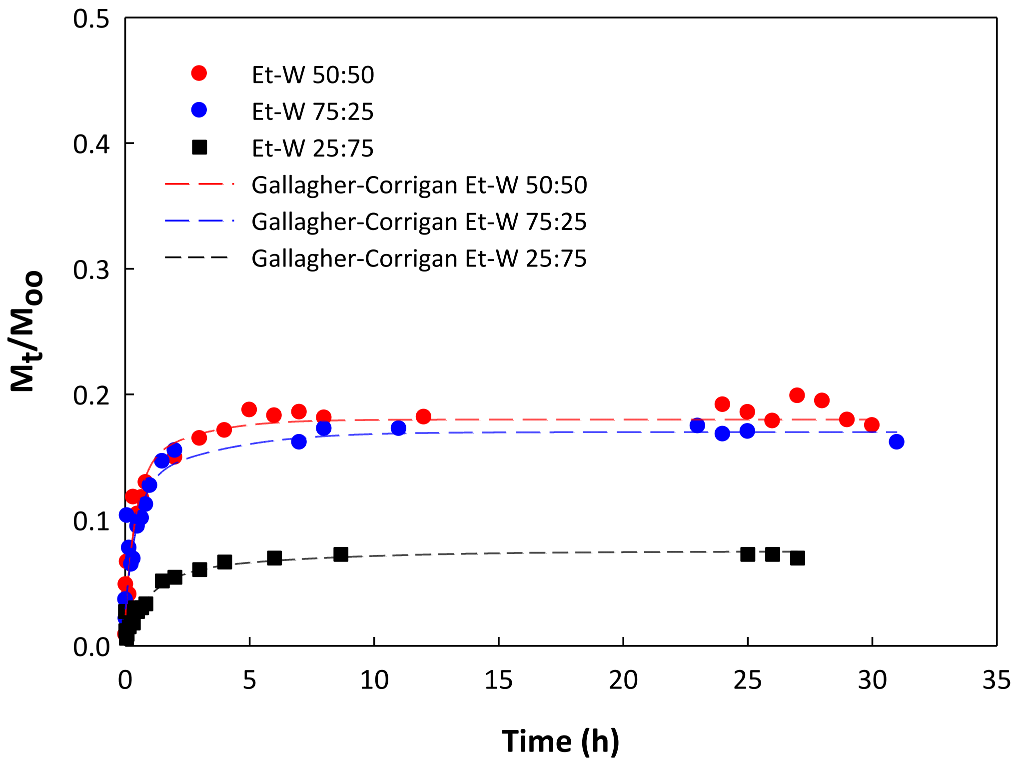

Figure 4. Controlled release of *Mentha piperita* essential oil in media with different percentages of ethanol: 75% (blue color), 50% (red color), and 25% (black color).

Data are the mean ± SD. of three repetitions (n = 3). References: Full-color symbol: experimental data, color solid line: Gallagher–Corrigan model fit.

According to Wang et al (2011), the incorporation of chitosan may decrease the amount of released oil due to interactions between the essential oils and the polymeric matrix.

To elucidate the mechanism of EO release, several semiempirical models were applied to experimental data. One of the most useful models to fill out this objective is the one proposed by Korsmeyer and Peppas (Peppas and Korsmeyer 1987), which describes the following equation:

$$\frac{M_t}{M_\infty} = k\,t^n \qquad [2]$$

Where M_t represents the amount of EO released at time t, M_∞ is the quantity of EO at infinite time, k is a transport constant (min^{-1}), and n is an adimensional parameter that describes the mechanism type. It is noteworthy that this model is only applicable in the time interval where the amount released was lower than 60%.

Table 5 summarizes the parameter values of the semi-empirical model proposed by Korsmeyer and Peppas. In this model, the constant k provides an estimation of the amount of active compound released from the polymeric matrix into the respective medium, reflecting a trend similar to that shown in Figure 5. Furthermore, this model facilitates an estimation of the transport process through the n constant, which depends on the geometry of the matrix (Peppas and Korsmeyer 1987; Siepmann and Peppas 2011). For cylindrical matrices, if n<0.45, the process is characterized as Fickian transport; if 0.45<n<0.89, it indicates non-Fickian transport, and if n>0.89, the predominant mechanism is erosion matrix. In the case of the matrix exposed to the 50% ethanol medium, the n value was found to be 0.68, while for media with 25% and 75% ethanol, n value was 0.52. This indicates that, in all instances, the release mechanism was governed by a dual mechanism that combined the Fickian diffusion and the matrix swelling.

To calculate the diffusion coefficient associated with controlled release, for a non-steady state, a trigonometric series was used (Lamarra et al., 2016).

$$\frac{M_t}{M_\infty} = 1 - \sum_{n=0}^{\infty} \frac{8}{(2n+1)^2\, 2n^2} \exp\left[-\frac{(2n+1)^2}{\delta^2} \pi^2 D t \right] \qquad [3]$$

being, M_t the total quantity of the substance that is released in time t, and M_∞ the corresponding quantity at an infinite time, D represents the diffusion coefficient, and delta is the electrospun mat thickness.

The analysis of the diffusion coefficient calculation revealed, as shown in Table 5, that this parameter significantly decreased when the solvent exhibited greater hydrophilicity. This observation suggested that the "*burst*" phase was governed by the polarity of the solvent, highlighting the critical role of the solubility of the EO in the media.

Table 5. Korsmeyer and Peppas model values, and diffusion coefficients of *Mentha piperita* in simulant media with different proportions of ethanol:water (Et-W)

Medium (ethanol-water)	Korsmeyer-Peppas			Diffusion coefficients
	K (min^{-1})	n	R^2	D ($cm^2\ s^{-1} \times 10^{-10}$)
75:25	0.12	0.52	0.9462	2.4
50:50	0.17	0.68	0.9469	2.3
25:75	0.037	0.52	0.965	0.25

The Gompertz model is an empirical exponential model, not deduced from any kinetic basis (Paarakh et al., 2018), where a and b are determined empirically by fitting the model to experimental data.

$$\frac{M_t}{M_\infty} = exp\left[-a \times exp(b \times log\,t)\right] \quad [4]$$

where, M_t/M_∞ is the percent of active agent released at time t, a parameter determines the undissolved proportion at t = 1 described as a location or scale parameter, b dissolution rate per unit of time describes a shape parameter.

The Gallagher and Corrigan model is one of the most suitable for describing the release mechanism in nanocomposite systems (Lamarra et al., 2020). This model proposes a combination of two phenomena, diffusion and degradation, which are detailed in the following equation:

$$F_t = F_b(1 - e^{-Kbt}) + (1 - F_b)\frac{e^{kt - kt\,max}}{1 + e^{kt - kt\,max}} \quad [5]$$

where Ft is the dosed amount of active compound at time t, Kb is the burst rate constant, Fb is the fraction of the active compound released in the burst phase, t_{max} is the time for maximum rate, and k is the rate constant of the polymer degradation phase.

Table 6 summarizes the parameters of different models.

Table 6. Parameters of the Gompertz and Gallagher-Corrigan models for controlled release of *Mentha piperita* in simulant media with different ethanol:water ratios obtained from the fitting of experimental data

Medium (ethanol-water)	**Gompertz**			**Gallagher and Corrigan**		
	a	**b**	**R^2**	**K_b (h^{-1})**	**k**	**R^2**
50:50	0.1760	0.2201	0.9730	2.2±0.3	0.6±0.3	0.9802
75:25	0.163	0.1967	0.9537	2.0±0.3	0.4±0.3	0.9556
25:75	0.0714	0.4880	0.9789	0.8±0.1	0.2±0.1	0.9713

Since the Gompertz model includes the b parameter as an indicator of the polymer dissolution rate over time, an increase in the medium´s polarity led to an increase in this parameter (Viscusi et al. 2023). These results were supported by the hydrophilicity of the primary polymer used in the matrix, which was PVA.

The dosage process was modeled employing a suitable kinetic model to describe the release behavior. In this sense, the model proposed by Gallagher and Corrigan was used, from which the parameters K_b and k were obtained. As shown in Table 6, this model provided a good fit for the experimental data. When examining the "*burst*" constant (K_b), the immersion media containing 50% and 75% ethanol did not exhibit significant differences ($p<0.05$). Conversely, the release in the solvent with greater hydrophilicity showed a significantly lower value ($p<0.05$). This result was supported by earlier discussions, reinforcing the hypothesis that the release during the "*burst*" phase was dependent on the polarity of the solvents. Focusing on the rate constant of the polymer degradation (k), the medium with 50% ethanol presented a higher value for this constant, reaffirming that both solvent polarity and matrix swelling play crucial roles in polymer dissolution. Similar results were reported by Fan et al. (2023), who investigated chitosan/gelatin films functionalized with zein-based Pickering emulsions loaded with cinnamon essential oil. These authors worked with two solvents (95% and 50% ethanol) and revealed that media with equivalent proportions of ethanol and water resulted in the highest concentration of EO released, suggesting that this medium disrupts the bilayer structure due to the polymer swelling. Thus, the biphasic release behavior described by the Gallagher and Corrigan model indicates that when $Kb > k$, the process is initially dominated by the EO diffusion during the burst phase, while the slower second phase is governed by swelling or relaxation of the polymeric electrospun matrix, enabling the sustained release of the entrapped active compound.

3.8 *In vitro* antimicrobial activity and spectroscopic insights

When *S. aureus* cultures were incubated at 20 °C in the presence of PVA/S or PVA/PE, statistically significant differences in microbial growth were observed between PVA/PE and PVA/S, as well as between PVA/PE and the control ($p<0.05$), with a lower number of microorganism in the presence of the PVA/PE mat at both 24 h and 48 h (Table 7).

In contrast, when *E. coli* cultures were incubated at 20 °C under the same conditions, no significant differences were found between PVA/S and PVA/PE at 48 h, although a trend ($p=0.07$) toward reduced growth was observed at 24 h with PVA/PE compared to PVA/S and the control.

In summary, statistical analysis evidenced that the differences among treatments were significant ($p<0.05$), as well as those observed between the evaluated times ($p<0.05$). Likewise, a significant interaction between treatment and time was detected ($p<0.05$), indicating that the effect of the treatments depends on the evaluation time, as can be seen in Table 7.

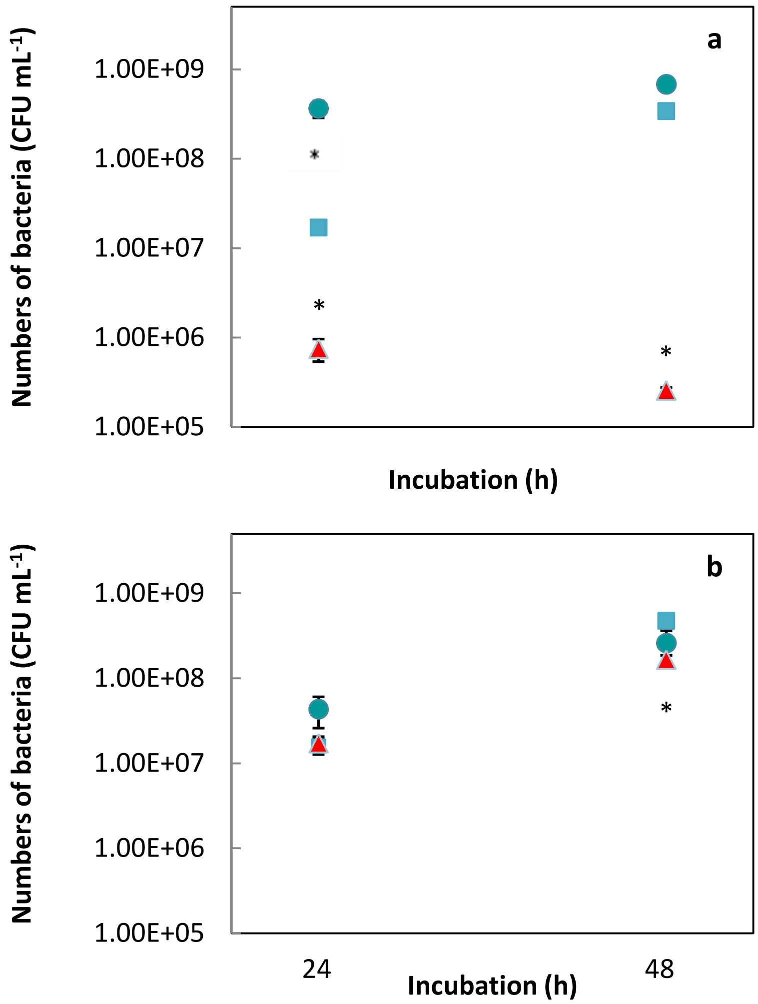

Figure 5. Bacterial count of *E. coli* (a) and *S. aureus* (b) incubated with electrospun mats (PVA/S and PVA/PE 4:1) at 30°C for 24 and 48 h. Data are presented as mean ± SD (n = 3), *$p < 0.05$.

Table 7. Antimicrobial activity of PCA/S and PCA/PE on *S. aureus* and *E. coli* at 20 °C for 24 and 48h. Data are presented as mean ± SD (n = 3)

	N° of bacteria (log CFU ml^{-1})			
	S. aureus		***E. coli***	
	24 h	**48 h**	**24 h**	**48 h**
Control	8.37^{c} ± 0.01	8.59^{d} ± 0.01	8.44^{c} ± 0.05	8.28^{b,c} ± 0.03
PVA/S	8.31^{c} ± 0.07	8.32^{c} ± 0.06	8.34^{b,c} ± 0.14	8.29^{b,c} ± 0.11
PVA/PE	7.40^{b} ± 0.12	6.70^{a}± 0.01	7.54^{a} ± 0.28	8.19^{b} ± 0.06

^{a,b,c} Different superscript letters within the same column indicate significant differences among the combinations of treatments (the tested films) and contact time with microorganisms (p < 0.05).

When assays were conducted at 30 °C, both strains reduced growth when bacteria were incubated with PVA/PE for 48 h (p<0.05) (Figure 5a and b), compared to PVA/S and control. Indeed, *S. aureus* showed a significant decrease at 24 h of incubation both in the presence of PVA/PE and PVA/S mats (p<0.05) (Figure 5b).

Several studies demonstrated that *Mentha sp.* has an antimicrobial effect on bacteria (Muntean et al, 2019; Mahboubi and Haghi, 2008; Silva et al., 2022). According to Kong et al. (2022) and Acevedo-Fani et al. (2015), the compounds present in the EO can disrupt the proteins structured in the membrane of microbial cells through hydrophobic interactions, altering membrane permeability. The major sensibility of *S. aureus* to the antimicrobial action of Mentha essential oil was reported previously (Muntean et al., 2019; Mahboubi and Haghi, 2008), related to differences in membrane composition that could produce different hydrophobic interactions.

Indeed, the results showed that antibacterial capacity increased with the temperature for both strains. This fact could be due to the increase in the active compound diffusion because of an increase in molecular kinetic energy (Xi et al., 2023).

The molecular interactions between the electrospun mats and bacterial strains were analyzed by ATR-FTIR (Figure 6). To interpret the complex biological material spectra, they can be divided into six spectral windows (Wi). W1.-3500–3100 cm^{-1} window corresponds to the presence of OH and NH, attributed to hydration of bacterial cells. W2.- 3000–2800 cm^{-1} exhibits the vibrations corresponding to C–H in the functional groups CH_3 and CH_2 (Naumann 2006).

W3.- 1800–1500 cm^{-1} called Amide I and II. W4.- 1300–1500 cm^{-1} involves functional groups present in lipids, proteins, carbohydrates, and nucleic acids. W5.-1200–900 cm^{-1}, dominated by symmetric stretching of the PO_2 group attributed to nucleic acids (1080 cm^{-1}) and phospholipids, and peaks due to various oligo and polysaccharides (Naumann 2006). W6.-900–750 cm^{-1} is the fingerprint region. In response to the stress induced by treatment with mats, the ATR-FTIR spectra of microorganism cells exhibited changes across several spectral windows, encompassing multiple of the aforementioned regions.

Modifications in the W1 and W2 regions were accompanied by a loss of definition of the peaks as can be observed in bands at 3600 and 3060 $cm^{-1,}$ indicating cellular membrane disruption (Cheng et al., 2023; Hayles et al., 2024). The amide II band at 1540 cm^{-1}, attributed to the N–H bending coupled to the C–N stretching of cell protein, became less sharp only in the case of *S. aureus*, remaining quasi-intact for *E. coli* incubated with mats without EO. Intensity reductions in this peak indicate modifications in the structure of transmembrane proteins (Zlotnikov et al., 2023).

Among spectral changes observed, signals associated with membrane phospholipids were identified. The peaks at 1235 cm^{-1} and 1076 cm^{-1}, reflecting asymmetric and symmetric phosphate stretching vibration, respectively, were altered after incubation of both microorganisms with PVA-based mats. Alterations in these bands may also indicate conformational changes in nucleic acids with modifications resulting from DNA damage and disruption of RNA functionality (Hayles et al., 2024).

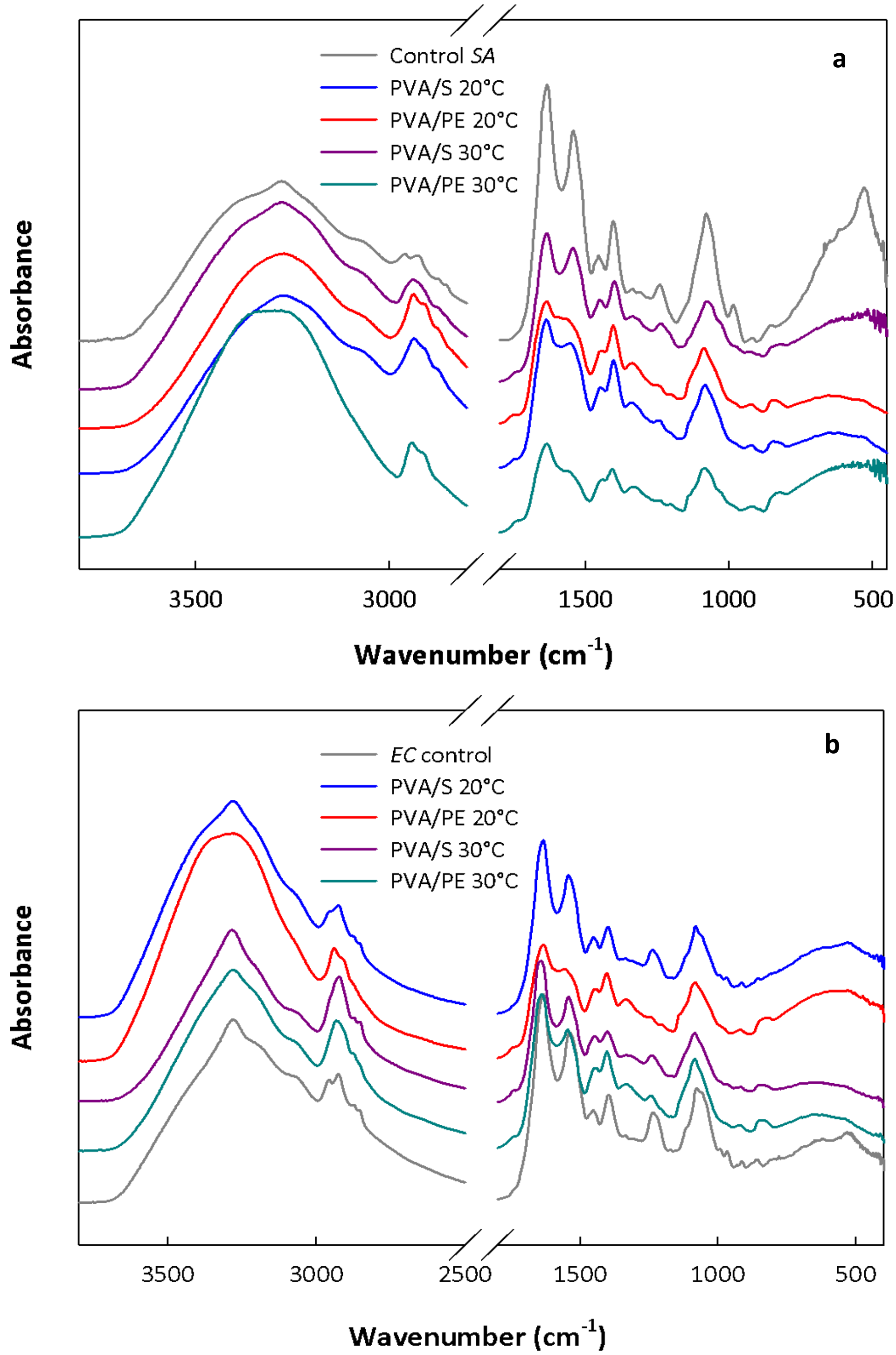

Figure 6. ATR-FTIR spectra of microorganisms incubated with electrospun mats at 20°C and 30°C for 24 hs: (**a**) *EC* control, without *Mentha piperita* PVA/S 4:1, and with *Mentha piperita* PVA/PE 4:1; **(b)** *SA* control, without *Mentha piperita* PVA/S 4:1, and with *Mentha piperita* PVA/PE 4:1. *E. coli* (*EC*), *S. aureus* (*SA*).

The modifications observed in the ATR-FTIR spectra are associated with the disruption of the bacterial membrane, which was more pronounced in *S. aureus,* Gram-positive bacteria that lack the outer membrane barrier found in Gram-negative bacteria. Although a similar trend was observed in both bacterial strains, *S. aureus* showed greater sensitivity to the electrospun mat. These facts could be sustained based on their bacterial classification: *S. aureus* is a Gram-positive bacterium, meanwhile *E. coli* is a Gram-negative bacterium with a double membrane with an outer layer composed of lipopolysaccharides, which prevents the penetration of active compounds (Unalan et al., 2019; Al-Sudani et al., 2024).

In addition, the effect of EO was linked to the menthol compound with the capacity to penetrate the bacterial membranes due to its hydrophobic character (Trombetta et al., 2005; Unalan et al., 2019; Vepštaitė-Monstavičė et al., 2023).

In addition, Hu et al. (2007) reported that the main alteration in the fatty acid region of the spectra of bacteria incubated with nanoparticles Ag/TiO_2 resulted in a reduction in the intensity of the peaks at 2872 and 2852 cm^{-1}.

After 48 h, the same trend was observed with major modifications in the presence of the EO, which was concordant with the count results.

3.9 Antimicrobial challenge: Food application of nanostructured active mat

The incorporation of EO into packaging containers to ensure and extend product shelf-life is referred to as active packaging (Kong et al., 2022). In this sense, the assays corresponding to the application of the material to ham samples showed that microbial growth inhibition was observed under the optimal growth conditions of microorganisms. Given that the inhibitory effect against *S. aureus* was promising and persisted up to 48 h, we proceeded to test the films in a real food application system. Ham was selected as the model food matrix because *S. aureus* is part of its typical microbiota. Incubations were performed at 4 °C, the standard storage temperature for ham.

After 48 h of incubation of the ham with the mats at 4 °C, a significant inhibition of *S. aureus* tellurite-positive growth was observed in the presence of PVA/PE mats compared to synthetic films (nylon) ($p<0.05$) (Figure 7). These findings suggest that the incorporation of chitosan may dose the amount of released oil due to interactions between the essential oils and the polymeric matrix, thereby maintaining a relatively high concentration of active compounds within the system and consequently enabling the prolonged maintenance of its antimicrobial activity (Wang et al., 2011).

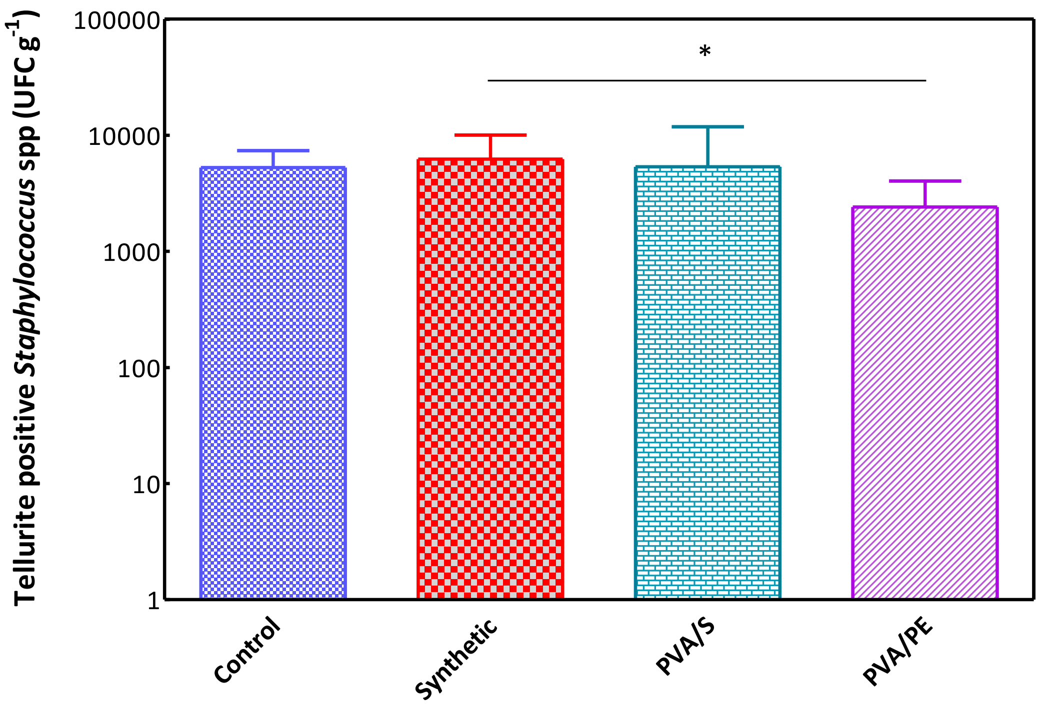

Figure 7. Bacterial count of *S. aureus* after 48 h of incubation of ham pieces with mats with and without *Mentha piperita* EO (PVA/PE 4:1 and PVA/S 4:1) at 4 °C, showing *S. aureus* tellurite-positive growth compared to synthetic films. * Means significant differences between treatment and control ($p < 0.05$).

It is noteworthy that PVA/S did not show significant differences when compared to the synthetic film (Figure 7).

Based on these results, the antibacterial activity the ham against *S. aureus* could be due to EO diffusion. These results were consistent with those reported by Djenane et al. (2012), who evaluated the bacterial growth of *E. coli* and *S. aureus* in minced beef against *Mentha piperita* EO, indicating a considerable reduction in log count of *S. aureus*. On the other hand, Šojić et al.

(2020) evaluated the antibacterial capacity of peppermint essential oil against *Listeria monocytogenes* (a Gram-positive bacterium) in cooked pork sausages, reporting a drastic reduction in bacterial count, indicating that this EO could replace the nitrite addition in this food.

CONCLUSIONS

Electrospun PVA-based nanofibers loaded with chitosan-stabilized *Pickering* emulsions encapsulating *Mentha piperita* essential oil were developed. The adequate rheological properties of the polymer solution provided predictive insight for evaluating its potential in the electrospinning process. The presence of the essential oil modified the microstructure, solubility, and mechanical properties of the PVA matrix.

Likewise, the polarity of release media influenced the liberation profile of the active agent. Diffusion and swelling mechanisms governed the liberation of *Mentha piperita*. The presence of the EO reduced the microbial count of *S. aureus* both *in vitro* and when applied to a ham-based food model, confirmed through ATR-FTIR studies. These results suggest the potential of these active materials as antimicrobial systems for food packaging, helping to enhance food safety and extend shelf-life.

Figure Captions

Figure 1. Dynamic rheology test of the samples: **a)** PVA solution, **b)** PVA/S 4:1 (without peppermint EO), **c)** PVA/PE 4:1, **d)** PVA/PE 3:1, and **e)** PVA/PE 2.5:1.

Figure 2. SEM micrographs of nanofibers formulated with: a) PVA, b) PVA/S 4:1, c) PVA/PE 4:1, d) PVA/PE 3:1, and e) PVA/PE 2.5:1. Magnification and average diameters (with the corresponding standard deviation) are indicated in the micrographs.

Figure 3. ATR-FTIR spectra of electrospun matrices functionalized with different proportions of *Mentha piperita* essential oil showing different regions: a) 3600 -3000 cm^{-1}, b) 3000-2700 cm^{-1}, and, c) 1150-950 cm^{-1}.

Figure 4. Controlled release of *Mentha piperita* essential oil in media with different percentages of ethanol: 75% (blue color), 50% (red color), and 25% (black color).

Data are the mean ± SD. of three repetitions (n = 3). References: Full-color symbol: experimental data, color solid line: Gallagher–Corrigan model fit.

Figure 5. Bacterial count of *E. coli* (a) and *S. aureus* (b) incubated with electrospun mats (PVA/S and PVA/PE 4:1) at 30°C for 24 and 48 h. Data are presented as mean ± SD (n = 3), *p < 0.05.

Figure 6. ATR-FTIR spectra of microorganisms incubated with electrospun mats at 20°C and 30°C for 24 hs: a) *EC* control, without *Mentha piperita* PVA/S 4/1, and with *Mentha piperita* PVA/PE 4:1; b) *SA* control, without *Mentha piperita* PVA/S 4/1, and with *Mentha piperita* PVA/PE 4:1. *E. coli* (*EC*), *S. aureus* (*SA*).

Figure 7. Bacterial count of *S. aureus* after 48 h of conservation of ham pieces with mats with and without *Mentha piperita* EO (PVA/PE 4:1 and PVA/S 4:1) at 4 °C, showing *S. aureus* tellurite-positive growth compared to synthetic films. *Means significant differences between treatment and control (p < 0.05).

Funding declaration

This work was supported by the National Scientific and Technical Research Council (CONICET) (Projects PIP 2023-00329 and PIP 2022-0493).

Authors acknowledge Pia Zarate for assistance in microbiological media preparation.

Author's contributions

JL: Methodology, investigation, formal analysis. JM: Methodology, investigation, data curation, writing-review. MM: Methodology, data curation and writing-review. DL: Conceptualization, formal analysis. SR: Conceptualization, writing-original draft, formal analysis, writing-review & editing, funding acquisition. AP: Conceptualization, writing-original draft, formal analysis, writing-review & editing, funding acquisition.

All the authors have approved the final version of the manuscript.

Declaration of conflicting interests

The authors declare no potential conflicts of interest concerning the research, authorship, and/or publication of this article.

Data availability

Data will be made available on request.

References

Acevedo-Fani, A., Salvia-Trujillo, L., Rojas-Graü, M. A., & Martín-Belloso, O. (2015). Edible films from essential-oil-loaded nanoemulsions: Physicochemical characterization and antimicrobial properties. *Food hydrocolloids*, *47*, 168-177. https://doi.org/10.1016/j.foodhyd.2015.01.032

Ahmed, R., Wang, M., Qi, Z., Hira, N. U. A., Jiang, J., Zhang, H., Iqbal, S., Wang, J., Cohen Stuart, M., A. & Guo, X. (2021). Pickering emulsions based on the pH-responsive assembly of food-grade chitosan. *ACS omega*, *6*(28), 17915-17922. https://doi.org/10.1021/acsomega.1c01490

Al-Sudani, B. T., Khoshkalampour, A., Kamil, M. M., Al-Musawi, M. H., Mohammadzadeh, V., Ahmadi, S., & Ghorbani, M. (2024). A novel antioxidant and antimicrobial food packaging based on Eudragit®/collagen electrospun nanofiber incorporated with bitter orange peel essential oil. Lwt, 193, 115730.https://doi.org/10.1016/j.lwt.2024.115730

Ardekani, N. T., Khorram, M., Zomorodian, K., Yazdanpanah, S., Veisi, H., &Veisi, H. (2019). Evaluation of electrospun poly (vinyl alcohol)-based nanofiber mats incorporated with Zataria multiflora essential oil as potential wound dressing. *International journal of biological macromolecules*, 125, 743-750.https://doi.org/10.1016/j.ijbiomac.2018.12.085

Ashrafudoulla, M., Mevo, S. I. U., Song, M., Chowdhury, M. A. H., Shaila, S., Kim, D. H., Nahar, S., Toushik, S.H.& Ha, S. D. (2023). Antibiofilm mechanism of peppermint essential oil to avert biofilm developed by foodborne and food spoilage pathogens on food contact surfaces. *Journal of Food Science*, 88(9), 3935-3955.https://doi.org/10.1111/1750-3841.16712.

Berton-Carabin, C. C., & Schroën, K. (2015). Pickering emulsions for food applications: background, trends, and challenges. *Annual review of food science and technology*, *6*(1), 263-297. https://doi.org/10.1146/annurev-food-081114-110822

Bezrodnykh, E. A., Antonov, Y. A., Berezin, B. B., Kulikov, S. N., & Tikhonov, V. E. (2021). Molecular features of the interaction and antimicrobial activity of chitosan in a solution containing sodium dodecyl sulfate. *Carbohydrate Polymers*, 270, 118352.https://doi.org/10.1016/j.carbpol.2021.118352

Çay, A., Miraftab, M., & Kumbasar, E. P. A. (2014). Characterization and swelling performance of physically stabilized electrospun poly (vinyl alcohol)/chitosan nanofibres. *European polymer journal*, *61*, 253-262. https://doi.org/10.1016/j.eurpolymj.2014.10.017

Chen, L., Liu, Z., Shi, J., Wang, C., Ding, L., Ding, X., Teng, G., Wu, J.& Zhang, J. (2022). Preparation and antibacterial properties of chitosan/polyvinyl alcohol nanofibrous mats using different organic acids as solvents. *Process Biochemistry*.https://doi.org/10.1016/j.procbio.2022.08.025

Cheng, Z. L., Qin, X. X., Liu, Z., & Qin, D. Z. (2017). Electrospinning preparation and mechanical properties of PVA/HNTs composite nanofibers. *Polymers for Advanced Technologies*, 28(6), 768-774.https://doi.org/10.1002/pat.3975

Cheng, C., Jiang, T., Zhang, D., Wang, H., Fang, T., & Li, C. (2023). Attachment characteristics and kinetics of biofilm formation by Staphylococcus aureus on ready-to-eat cooked beef contact surfaces. Journal of Food Science, 88(6), 2595-2610.

Costa, A. L. R., Gomes, A., & Cunha, R. L. (2018). One-step ultrasound producing O/W emulsions stabilized by chitosan particles. *Food research international,* 107, 717-725.https://doi.org/10.1016/j.foodres.2018.02.057

Das, K. P., Singh, P., & Satapathy, B. K. (2023). Nanofibrous-substrate-based controlled herbicidal release systems: Atrazine/hydroxypropyl-β-cyclodextrin inclusion complex loaded PVA agro-augmenting electrospun mats*. Journal of Environmental Chemical Engineering*, 11(6), 111586.https://doi.org/10.1016/j.jece.2023.111586

de Oliveira Mori, C. L., dos Passos, N. A., Oliveira, J. E., Mattoso, L. H. C., Mori, F. A., Carvalho, A. G., de Souza Fonseca, A., & Tonoli, G. H. D. (2014). Electrospinning of zein/tannin bio-nanofibers. *Industrial Crops and Products*, *52*, 298-304. https://doi.org/10.1016/j.indcrop.2013.10.047

Djenane, D., Aïder, M., Yangüela, J., Idir, L., Gómez, D., Roncalés, P. (2012). Antioxidant and antibacterial effects of Lavandula and Mentha essential oils in minced beef inoculated with E. coli O157: H7 and S. aureus during storage at abuse refrigeration temperature. *Meat science*, 92(4), 667-674.https://doi.org/10.1016/j.meatsci.2012.06.019

Erdem, R., & Akalın, M. (2015). Characterization and evaluation of antimicrobial properties of electrospun chitosan/polyethylene oxide based nanofibrous scaffolds (with/without nanosilver*). Journal of Industrial Textiles*, 44(4), 553-571. DOI: 10.1177/1528083713503000

Fan, S., Wang, D., Wen, X., Li, X., Fang, F., Richel, A., Xia, N., Fauconnier, M-L., Hou, C. & Zhang, D. (2023). Incorporation of cinnamon essential oil-loaded Pickering emulsion for improving antimicrobial properties and control release of chitosan/gelatin films. *Food Hydrocolloids*, 138, 108438. https://doi.org/10.1016/j.foodhyd.2022.108438

Fasihi, H., Noshirvani, N., & Hashemi, M. (2023). Novel bioactive films integrated with Pickering emulsion of ginger essential oil for food packaging application. *Food Bioscience*, 51, 102269.https://doi.org/10.1016/j.fbio.2022.102269

Gaikwad, K. K., Singh, S., & Ajji, A. (2019). Moisture absorbers for food packaging applications. *Environmental Chemistry Letters*, *17*(2), 609-628. https://doi.org/10.1007/s10311-018-0810-z

Gahruie, H. H., Ziaee, E., Eskandari, M. H., & Hosseini, S. M. H. (2017). Characterization of basil seed gum-based edible films incorporated with Zataria multiflora essential oil nanoemulsion. *Carbohydrate polymers*, *166*, 93-103. https://doi.org/10.1016/j.carbpol.2017.02.103

Garavand, Y., Taheri-Garavand, A., Garavand, F., Shahbazi, F., Khodaei, D., & Cacciotti, I. (2022). Starch-polyvinyl alcohol-based films reinforced with chitosan nanoparticles: physical, mechanical, structural, thermal and antimicrobial properties. *Applied Sciences*, *12*(3), 1111. https://doi.org/10.3390/app12031111

Hadidi, M., Pouramin, S., Adinepour, F., Haghani, S., & Jafari, S. M. (2020). Chitosan nanoparticles loaded with clove essential oil: Characterization, antioxidant and antibacterial activities. *Carbohydrate polymers*, *236*, 116075. https://doi.org/10.1016/j.carbpol.2020.116075

Hayles, A., Bright, R., Nguyen, N. H., Truong, V. K., Vongsvivut, J., Wood, J.,Kidd, S.P.& Vasilev, K. (2024). Staphylococcus aureus surface attachment selectively influences tolerance against charged antibiotics. *Acta Biomaterialia*, 175, 369-381.https://doi.org/10.1016/j.actbio.2023.12.029

Hu, C., Guo, J., Qu, J., & Hu, X. (2007). Photocatalytic degradation of pathogenic bacteria with AgI/TiO2 under visible light irradiation. *Langmuir*, *23*(9), 4982-4987. https://doi.org/10.1021/la063626x

Javaid, A., Jalalah, M., Safdar, R., Khaliq, Z., Qadir, M. B., Zulfiqar, S., Ahmad A., Satti A. N., Ali, A., Faisal, M., Alsareii S., A. & Harraz, F. A. (2022). Ginger Loaded Polyethylene Oxide Electrospun Nanomembrane: Rheological and Antimicrobial Attributes. *Membranes*, 12(11), 1148. https://doi.org/10.3390/membranes12111148

Jiang, T., Wang, D., Zhang, X., Yang, Q., Huang, Q., Ju, X., Li, L., Kang, X.& Li, C. (2024). Electrospinning of chitosan/polyvinyl alcohol Pickering emulsion with tea tree essential oil loaded for anti-infection wound dressings*.* *Materials Chemistry and Physics*, 311, 128561.https://doi.org/10.1016/j.matchemphys.2023.128561

Kamatou, G. P., Vermaak, I., Viljoen, A. M., & Lawrence, B. M. (2013). Menthol: A simple monoterpene with remarkable biological properties. *Phytochemistry*, *96*, 15-25. https://doi.org/10.1016/j.phytochem.2013.08.005

Kavoosi, G., Rahmatollahi, A., Dadfar, S. M. M., &Purfard, A. M. (2014). Effects of essential oil on the water binding capacity, physico-mechanical properties, antioxidant and antibacterial activity of gelatin films. *LWT-Food Science and Technology*, 57(2), 556-561.https://doi.org/10.1016/j.lwt.2014.02.008

Kong, I., Degraeve, P., & Pui, L. P. (2022). Polysaccharide-based edible films incorporated with essential oil nanoemulsions: Physico-chemical, mechanical properties and its application in food preservation—A review. *Foods*, *11*(4), 555. https://doi.org/10.3390/foods11040555

Lai, H., Liu, Y., Huang, G., Chen, Y., Song, Y., Ma, Y., & Yue, P. (2021). Fabrication and antibacterial evaluation of peppermint oil-loaded composite microcapsules by chitosandecorated silica nanoparticles stabilized Pickering emulsion templating. *International Journal of Biological Macromolecules*, *183*, 2314-2325. https://doi.org/10.1016/j.ijbiomac.2021.05.198

Lamarra, J., Rivero, S., & Pinotti, A. (2016). Design of chitosan-based nanoparticles functionalized with gallic acid. *Materials Science and Engineering: C*, 67, 717-726.https://doi.org/10.1016/j.msec.2016.05.072

Lamarra, J., Calienni, M. N., Rivero, S., & Pinotti, A. (2020). Electrospun nanofibers of poly (vinyl alcohol) and chitosan-based emulsions functionalized with cabreuva essential oil. *International Journal of Biological Macromolecules*, 160, 307-318. https://doi.org/10.1016/j.ijbiomac.2020.05.096

Lamarra, J., Rivero, S., & Pinotti, A. (2022). Functionalized biomaterials based on poly (vinyl alcohol) and chitosan as a vehicle for controlled release of cabreuva essential oil. *Polymer Engineering & Science*.https://doi.org/10.1002/pen.26062

Lamarra, J., Rivero, S., Pinotti, A., & Lopez, D. (2023). Nanofiber mats functionalized with Mentha piperita essential oil stabilized in a chitosan-based emulsion designed via an electrospinning technique. *International Journal of Biological Macromolecules*, *248*, 125980. https://doi.org/10.1016/j.ijbiomac.2023.125980

Leung, Y. H., Xu, X., Ma, A. P., Liu, F., Ng, A. M., Shen, Z., Ghetings, L., A., Guo, M., U., Djurišić, A., B., Lee, P., K., H., Lee, H., K., Chan, W., K. & Leung, F. C. (2016). Toxicity of ZnO and TiO2 to Escherichia coli cells. *Scientific reports*, *6*(1), 35243. DOI: 10.1038/srep35243

Liguori, A., Pandini, S., Rinoldi, C., Zaccheroni, N., Pierini, F., Focarete, M. L., & Gualandi, C. (2022). Thermoactive smart electrospun nanofibers. *Macromolecular Rapid Communications*, *43*(5), 2100694. https://doi.org/10.1002/marc.202100694

Liu, X., Baldursdottir, S. G., Qu, H., Christensen, L. P., Rantanen, J., & Yang, M. (2015). Investigation of the correlation between electrospinnability and rheology. *Nordic Rheology Society Annual Transactions*, *23*, 225-229.

Liu, Z., Ramakrishna, S., Ahmed, I., Rudd, C., & Liu, X. (2022). Rheological, surface tension and conductivity insights on the electrospinnability of poly (lactic-co-glycolic acid)-hyaluronic acid solutions and their correlations with the nanofiber morphological characteristics. *Polymers*, *14*(20), 4411. https://doi.org/10.3390/polym14204411

Low, L. E., Siva, S. P., Ho, Y. K., Chan, E. S., & Tey, B. T. (2020). Recent advances of characterization techniques for the formation, physical properties and stability of Pickering emulsion. *Advances in colloid and interface science*, 277, 102117.https://doi.org/10.1016/j.cis.2020.102117

Mahboubi, M., & Haghi, G. (2008). Antimicrobial activity and chemical composition of Mentha pulegium L. essential oil. *Journal of ethnopharmacology*, *119*(2), 325-327. https://doi.org/10.1016/j.jep.2008.07.023

Milanesi, G., Vigani, B., Rossi, S., Sandri, G., & Mele, E. (2021). Chitosan-coated poly (lactic acid) nanofibres loaded with essential oils for wound healing. *Polymers*, 13(16), 2582. https://doi.org/10.3390/polym13162582

Mirres, A. C. D. M., Vieira, I. R. S., Tessaro, L., da Silva, B. D., de Andrade, J. C., da Silva, A. A.,Carvalho, N.F.M., Furtado de Sousa, A.M.& Conte-Junior, C. A. (2024). Nanocomposite Films of Babassu Coconut Mesocarp and Green ZnO Nanoparticles for Application in Antimicrobial Food Packaging. *Foods*, 13(12), 1895. https://doi.org/10.3390/foods13121895

Morais, M. S., Bonfim, D. P., Aguiar, M. L., & Oliveira, W. P. (2023). Electrospun Poly (Vinyl Alcohol) Nanofibrous Mat Loaded with Green Propolis Extract, Chitosan and Nystatin as an Innovative Wound Dressing Material. *Journal of Pharmaceutical Innovation*, 1-15. https://doi.org/10.1007/s12247-022-09681-7

Mouhoub, A., Raouan, S. E., Guendouz, A., El Alaoui-Talibi, Z., Koraichi, S. I., El Abed, S., Delattre, C., & El Modafar, C. (2022). Antiadhesion effect of the chitosan-based film incorporated with essential oils against foodborne bacteria. *Industrial Crops and Products*, *189*, 115742. https://doi.org/10.1016/j.indcrop.2022.115742Nadaf, A., Gupta, A., Hasan, N., Ahmad, S., Kesharwani, P., & Ahmad, F. J. (2022). Recent update on electrospinning and electrospun nanofibers: current trends and their applications. *RSC advances*, 12(37), 23808-23828.DOI: 10.1039/D2RA02864F

Muntean, D., Licker, M., Alexa, E., Popescu, I., Jianu, C., Buda, V., Dehelan, C.A., Ghiulai, R., Horhat, F., Horhat, D., & Danciu, C. (2019). Evaluation of essential oil obtained from Mentha× piperita L. against multidrug-resistant strains. *Infection and Drug Resistance*, 2905-2914. https://doi.org/10.2147/IDR.S218141

Naumann, D. (2006). Infrared spectroscopy in microbiology. *Encyclopedia of Ananlytical Chemistry.* https://doi.org/10.1002/9780470027318.a0117

Niu, B., Chen, H., Wu, W., Fang, X., Mu, H., Han, Y., & Gao, H. (2022). Co-encapsulation of chlorogenic acid and cinnamaldehyde essential oil in Pickering emulsion stablized by chitosan nanoparticles. *Food Chemistry: X*, 14, 100312.https://doi.org/10.1016/j.fochx.2022.100312

Paarakh, M. P., Jose, P. A., Setty, C. M., & Peterchristoper, G. V. (2018). Release kinetics–concepts and applications. *International Journal of Pharmacy Research & Technology (IJPRT)*, *8*(1), 12-20.

Panda, P. K., Sadeghi, K., & Seo, J. (2022). Recent advances in poly (vinyl alcohol)/natural polymer based films for food packaging applications: A review. *Food Packaging and Shelf Life*, 33, 100904.https://doi.org/10.1016/j.fpsl.2022.100904

Peppas, N. A., & Korsmeyer, R. W. (1987). Dynamically swelling hydrogels in controlled release applications. *Hydrogels in medicine and pharmacy*, *3*, 109-136.

Perez-Calderon, J., Marin-Silva, D. A., Zaritzky, N., &Pinotti, A. (2023). Eco-friendly PVA-chitosan adsorbent films for the removal of azo dye Acid Orange 7: Physical cross-linking, adsorption process, and reuse of the material. *Advanced industrial and engineering polymer research*, 6(3), 239-254.https://doi.org/10.1016/j.aiepr.2022.12.001

Piorkowski, D. T., & McClements, D. J. (2014). Beverage emulsions: Recent developments in formulation, production, and applications. *Food hydrocolloids*, 42, 5-41.https://doi.org/10.1016/j.foodhyd.2013.07.009

Ran, R., Zheng, T., Tang, P., Xiong, Y., Yang, C., Gu, M., & Li, G. (2023). Antioxidant and antimicrobial collagen films incorporating Pickering emulsions of cinnamon essential oil for pork preservation. *Food Chemistry*, 420, 136108.https://doi.org/10.1016/j.foodchem.2023.136108

Salaris, V., Leonés, A., Lopez, D., Kenny, J. M., & Peponi, L. (2022). Shape-memory materials via electrospinning: A review. *Polymers*, *14*(5), 995. https://doi.org/10.3390/polym14050995

Serpelloni, S., Williams, M. E., Caserta, S., Sharma, S., Rahimi, M., &Taraballi, F. (2024). Electrospun Chitosan-Based Nanofibrous Coating for the Local and Sustained Release of Vancomycin. *ACS omega*, 9(10), 11701-11717. https://pubs.acs.org/doi/10.1021/acsomega.3c08113.

Sharkawy, A., Barreiro, M. F., & Rodrigues, A. E. (2020). Chitosan-based Pickering emulsions and their applications: A review. *Carbohydrate Polymers*, 250, 116885. https://doi.org/10.1016/j.carbpol.2020.116885

Silva, W. M. F., Bona, N. P., Pedra, N. S., Cunha, K. D., Fiorentini, A. M., Stefanello, F. M., Zavareze, E., R., & Dias, A. R. G. (2022). Risk assessment of in vitro cytotoxicity, antioxidant and antimicrobial activities of Mentha piperita L. essential oil. *Journal of Toxicology and Environmental Health, Part A*, *85*(6), 230-242. https://doi.org/10.1080/15287394.2021.1999875

Siepmann, J., & Peppas, N. A. (2011). Higuchi equation: Derivation, applications, use and misuse. *International journal of pharmaceutics*, 418(1), 6-12. https://doi.org/10.1016/j.ijpharm.2011.03.051

Šojić, B., Pavlić, B., Tomović, V., Kocić-Tanackov, S., Đurović, S., Zeković, Z., Belović,M., Torbica, A., Jokanović, M., Urumović, N., Vujadinović, D., Ivić, M.&Škaljac, S. (2020). Tomato pomace extract and organic peppermint essential oil as effective sodium nitrite replacement in cooked pork sausages. *Food Chemistry*, 330, 127202.https://doi.org/10.1016/j.foodchem.2020.127202

Soltanbeigi, A., Özgüven, M., & Hassanpouraghdam, M. B. (2021). Planting-date and cutting-time affect the growth and essential oil composition of Mentha piperita and Mentha arvensis. *Industrial Crops and Products*, 170, 113790.https://doi.org/10.1016/j.indcrop.2021.113790

Tampau, A., González-Martínez, C., Chiralt, A. (2020). Polyvinyl alcohol-based materials encapsulating carvacrol obtained by solvent casting and electrospinning. *Reactive and Functional Polymers*, *153*, 104603. https://doi.org/10.1016/j.reactfunctpolym.2020.104603

Taylan, O., Cebi, N., & Sagdic, O. (2021). Rapid screening of mentha spicata essential oil and l-menthol in mentha piperita essential oil by atr-ftir spectroscopy coupled with multivariate analyses. *Foods*, 10(2), 202. https://doi.org/10.3390/foods10020202

Trombetta, D., Castelli, F., Sarpietro, M. G., Venuti, V., Cristani, M., Daniele, C., ... & Bisignano, G. (2005). Mechanisms of antibacterial action of three monoterpenes. Antimicrobial agents and chemotherapy, 49(6), 2474-2478.

Tu, W. X., Zuo, X. B., & Liu, H. F. (2008). Study on the interaction between polyvinylpyrrolidone and platinum metals during the formation of the colloidal metal nanoparticles. *Chinese Journal of Polymer Science*, *26*(01), 23-29. https://doi.org/10.1142/S0256767908002625

Unalan, I., Slavik, B., Buettner, A., Goldmann, W. H., Frank, G., &Boccaccini, A. R. (2019). Physical and antibacterial properties of peppermint essential oil loaded poly (ε-caprolactone)(PCL) electrospun fiber mats for wound healing. *Frontiers in Bioengineering and Biotechnology*, 7, 346.https://doi.org/10.3389/fbioe.2019.00346

Vahedikia, N., Garavand, F., Tajeddin, B., Cacciotti, I., Jafari, S. M., Omidi, T., & Zahedi, Z. (2019). Biodegradable zein film composites reinforced with chitosan nanoparticles and cinnamon essential oil: Physical, mechanical, structural and antimicrobial attributes. *Colloids and Surfaces B: Biointerfaces*, *177*, 25-32. https://doi.org/10.1016/j.colsurfb.2019.01.045

Vepštaitė-Monstavičė, I., Ravoitytė, B., Būdienė, J., Valys, A., Lukša, J., &Servienė, E. (2023). Essential oils of Mentha arvensis and Cinnamomum cassia exhibit distinct antibacterial activity at different temperatures in vitro and on chicken skin. *Foods*, 12(21), 3938. https://doi.org/10.3390/foods12213938

Viscusi, G., Paolella, G., Lamberti, E., Caputo, I., & Gorrasi, G. (2023). Quercetin-loaded polycaprolactone-polyvinylpyrrolidone electrospun membranes for health application: Design, characterization, modeling and cytotoxicity studies. Membranes, 13(2), 242. https://doi.org/10.3390/membranes13020242

Wang, L., Liu, F., Jiang, Y., Chai, Z., Li, P., Cheng, Y., Jing, H., & Leng, X. (2011). Synergistic antimicrobial activities of natural essential oils with chitosan films. *Journal of agricultural and food chemistry*, *59*(23), 12411-12419. dx.doi.org/10.1021/jf203165k

Wu, J., & Ma, G. H. (2016). Recent studies of Pickering emulsions: particles make the difference. *Small*, 12(34), 4633-4648. https://doi.org/10.1002/smll.201600877

Wu, X., Hu, Q., Liang, X., Chen, J., Huan, C., & Fang, S. (2022). Methyl jasmonate encapsulated in protein-based nanoparticles to enhance water dispersibility and used as coatings to improve cherry tomato storage. *Food Packaging and Shelf Life*, 33, 100925. https://doi.org/10.1016/j.fpsl.2022.100925

Wu, Y., Du, J., Zhang, J., Li, Y., &Gao, Z. (2023). pH Effect on the Structure, Rheology, and Electrospinning of Maize Zein. *Foods*, 12(7), 1395.https://doi.org/10.3390/foods12071395

Xi, X., Huang, J., Zhang, S., Lu, Q., Fang, Z., Li, C., Zhang, Q., Liu, Y., Chen, H., Liu, A., Wang, C., Li, S.& Hu, B. (2023). Preparation and characterization of inclusion complex of Myristica fragrans Houtt.(nutmeg) essential oil with 2-hydroxypropyl-β-cyclodextrin. *Food Chemistry*, *423*, 136316.

Zhang, Q., Lin, J., Dong, Y., & Sun, F. (2023). Investigation of the rheological response of a bio-liquefied formaldehyde resin-based precursor for electrospinning. *Colloids and Surfaces A: Physicochemical and Engineering Aspects*, 661, 130950.https://doi.org/10.1016/j.colsurfa.2023.130950

Zlotnikov, I. D., Ezhov, A. A., Vigovskiy, M. A., Grigorieva, O. A., Dyachkova, U. D., Belogurova, N. G., & Kudryashova, E. V. (2023). Application prospects of FTIR spectroscopy and CLSM to monitor the drugs interaction with bacteria cells localized in macrophages for diagnosis and treatment control of respiratory diseases. *Diagnostics*, 13(4), 698. https://doi.org/10.3390/diagnostics13040698

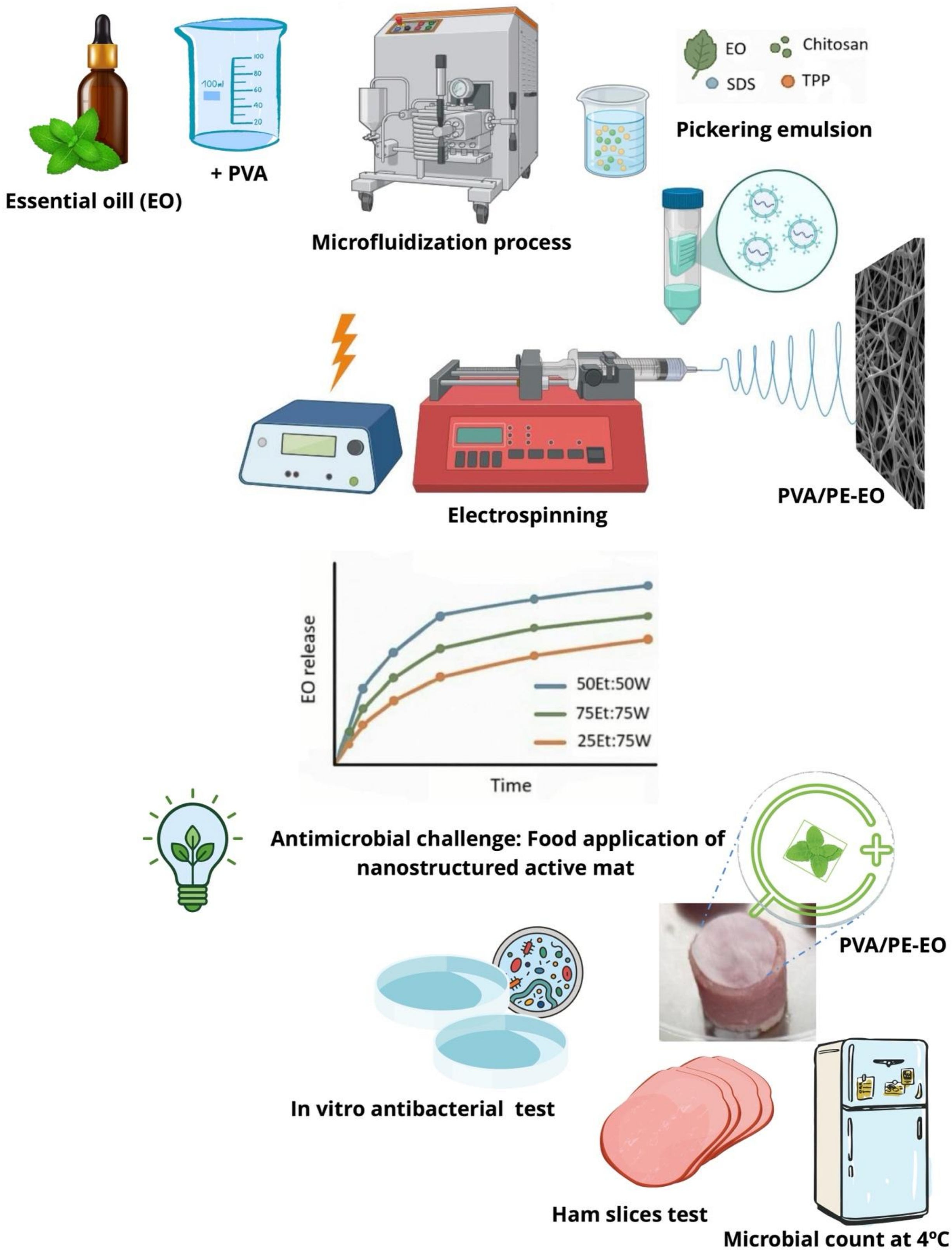

Lamarra et al. Graphical abstract